[redacted]

UNCLASSIFIED

LAMS-2688 C.3

Copy No. [redacted]

AEC RESEARCH AND DEVELOPMENT REPORT

LOS ALAMOS SCIENTIFIC LABORATORY

OF THE UNIVERSITY OF CALIFORNIA ○ LOS ALAMOS NEW MEXICO

[illegible]

A FEASIBILITY STUDY OF THE DISPOSAL OF A ROVER REACTOR WITH HIGH EXPLOSIVES

(Title Unclassified)

UNCLASSIFIED

[redacted]

LEGAL NOTICE

This report was prepared as an account of Government sponsored work. Neither the United States, nor the Commission, nor any person acting on behalf of the Commission:

A. Makes any warranty or representation, expressed or implied, with respect to the accuracy, completeness, or usefulness of the information contained in this report, or that the use of any information, apparatus, method, or process disclosed in this report may not infringe privately owned rights; or

B. Assumes any liabilities with respect to the use of, or for damages resulting from the use of any information, apparatus, method, or process disclosed in this report.

As used in the above, "person acting on behalf of the Commission" includes any employee or contractor of the Commission, or employee of such contractor, to the extent that such employee or contractor of the Commission, or employee of such contractor prepares, disseminates, or provides access to, any information pursuant to his employment or contract with the Commission, or his employment with such contractor.

Printed in USA. Charge $ 2.45. Available from the U.S. Atomic Energy Commission, Technical Information Service Extension, P. O. Box 1001, Oak Ridge, Tennessee. Please direct to the same address inquiries covering the procurement of other classified AEC reports.

[redacted]

LAMS-2688
C-91 NUCLEAR REACTORS
FOR ROCKET PROPULSION
M-3679 (26th Ed.)

This document consists of 97 pages
No. [redacted] of 135 copies, Series A

LOS ALAMOS SCIENTIFIC LABORATORY
OF THE UNIVERSITY OF CALIFORNIA LOS ALAMOS NEW MEXICO

REPORT WRITTEN: March 1962

REPORT DISTRIBUTED: July 3, 1962

A FEASIBILITY STUDY OF THE DISPOSAL OF A ROVER REACTOR WITH HIGH EXPLOSIVES

(Title Unclassified)

by

Jerry Wackerle

with Appendix B by

J. N. Fritz

[redacted]

[redacted]

ABSTRACT

This study examines the feasibility of utilizing a high explosive charge projected into a NERVA engine core to reduce it to small fragments for safety purposes. The technique described involves explosively reducing a number of scale-model configurations, varying in certain properties from shot to shot. The influence of these properties on obtained or expected fragment sizes is compared through the use of empirical distribution expressions. Certain conclusions are presented regarding the effects of scaling, explosive type and weight, graphite physical properties, geometrical configurations, and metal parts. Some rough estimates of fragment distributions anticipated in actual devices are given. Data related to the dispersal of engine parts in firing pad accidents, and some basic theoretical consideration of the expected form of the fragment-size distribution are given in Appendixes A and B.

UNCLASSIFIED

UNCLASSIFIED

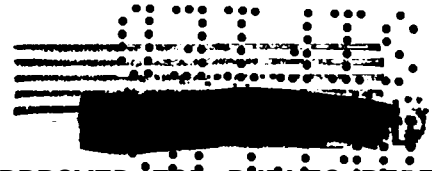

CONTENTS

I. INTRODUCTION

Among the various safety aspects associated with the flight of nuclear rocket engines are problems which arise from combining the potentially supercritical and radioactive features of the reactor core with the possibility of failure to achieve a desired orbit in a flight mission. Two primary problems which could result from the uncontrolled return of a nuclear-powered vehicle to earth are as follows:

1. In the event that before a run the reflector-controlled reactor should be suddenly immersed in water, it could become supercritical and explode in the manner of a small nuclear device. Estimates[1] of the "maximum credible accident" possible from such an event correspond to the detonation of a few tons of TNT. It is supposed that the explosion could be prevented by separation of the reactor core into about ten pieces prior to immersion.

1. LA-2409, "Nuclear Safety Aspects of the Rover Program," Appendix III (March, 1960)(SECRET).

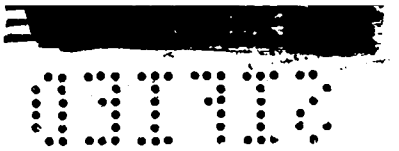

2. The high density of fission products in the reactor core after a run makes even small pieces of it potentially hazardous to the general population. Thus the possibility of a mission failure in which the vehicle fails to achieve orbit after a run requires a tolerable method for return of the core pieces to earth. The ideal solution would be some mechanism which would so finely divide the graphite material that it would remain suspended in the upper atmosphere or burn up on reentry. If this could not be accomplished, it would at least be desirable to disperse the core in fragments sufficiently small to be an acceptable hazard.

Just what size fragments could be permitted is a complicated question involving their residual radioactivity, decay and other factors; at present no criteria have been specified. Estimates of acceptable size have ranged as low as submillimeter. The investigation described in this report is not concerned with the size of fragments that could be permitted, but rather considers what sizes can be achieved with a certain mechanism. Obviously, a fragmentation method which would solve the second problem listed above should be quite adequate for the first. Consequently, this study has been directed toward the disposal of the reactor at high altitudes.

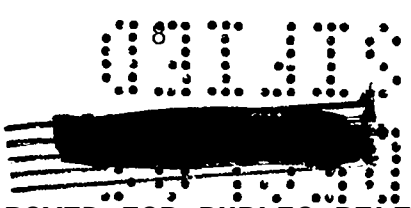

In the summer of 1961 a program was initiated to determine the feasibility of employing high explosives to dispose of a nuclear rocket engine. The concept of the particular manner in which explosives would be employed has been limited to a single mechanism. This mechanism is based on the idea of carrying in the NERVA vehicle a device which in a destruct situation would project a high-explosive shell into the engine. Such an arrangement resulted from the expected difficulties in having high explosive adjacent to the reactor during the run. Without an elaborate shielding and cooling system, the high neutron and gamma-ray flux would certainly alter the properties of the explosive, and could result in its undesired initiation.

The basic approach of the study, which is detailed in Section II, has been constructed around the fragmentation of scaled cylindrical graphite configurations (representing to greater or lesser extent actual Kiwi designs) with axially located, cylindrical explosive charges. The design of the models was to a large extent dictated by the type and shape of graphite materials which were quickly and economically available. The experimental program discussed in Section III proceeded in two phases. The first employed a so-called dispersal-recovery technique, to obtain

information on the size of fragments produced in a given configuration and the manner in which they were scattered by the explosion. The dispersal information, which could prove of use to those concerned with firing-pad accidents, such as a nuclear incident or the explosion of a chemical booster, is presented in Appendix A. The recovery data of this phase, while not as helpful as that obtained with later techniques, were sufficient to give an approximate idea of the fragmentation which could be accomplished with a reasonable amount of high explosive. Fragments recovered were small enough (tens of grams maximum size) to prove, when coupled with other factors, sufficiently promising[2] to lead to the second phase of the program. In that part, less realistic models were fired to see how various parameters, e.g., scaling or explosive/graphite weight ratios, might affect and optimize fragment size. The deductions, given in Section IV, were made on a strictly empirical comparison basis.

Section V contains a rough estimate of the degree of fragmentation which would occur in an actual reactor destroyed by 100 lb. of high explosive. Some conclusions and suggestions for further investigation are presented in Section VI.

2. Certainly graphite pieces of the order of tens of grams would be sufficiently radioactive to be a serious hazard; however present feeling is that fragments of such dimensions would be vaporized on reentry. Plasma jet experiments are underway to help determine how large a fragment may be permitted.

II. BASIC APPROACH OF THE STUDY

A purely hydrodynamic computation of fragmentation of an object by detonation of a centrally located explosive charge is a problem of virtually insolvable complexity. The complexity is magnified in this study by the fact that it deals with a material of ill-defined shock wave properties in a complicated geometrical configuration. Therefore, the approach in this program has been an empirical parameter study.

Since it is not known when and where a piece breaks in the explosion process, it is simply admitted that the process produces a collection of fragments of varying sizes. It is assumed that the performing of identical experiments dealing with a large number of fragments will lead to the recovery of identical distributions. These distributions may then be fit to mathematical expressions which incorporate certain parameters, and the variations of the parameters can be observed as certain aspects of the experiment are changed. If enough experiments are performed, and the

parameters of the fragment distribution function are found to vary in a consistent fashion, predictions should be possible for the destruction of an object not available for an experimental test, a class of objects which presently includes a full-scale Rover reactor.

The important aspects of the experiments which were varied in this program were:

1. Explosive-to-graphite mass ratio
2. Explosive type
3. Scale
4. Physical and mechanical properties of the graphite
5. Geometrical configurations
6. Presence of metal parts

The study of the parameters was made by the direct comparison of groups of shots in which (usually) only one of the above conditions was varied. A detailed discussion of the comparisons, and the conclusions drawn from them, appears in Section IV.

The expression employed to fit the fragment data is known as Rosin's Law.[3] If we define the incremental mass fraction of fragments having dimensions between R and R + dR as (dF/dR)dR, then Rosin's Law may be written:

3. R. J. Finkelstein and G. Gamow; "Theory of the Detonation Process," NAVORD Report 90-46 April, 1947)(CONFIDENTIAL).

$$(dF/dR)\,dR = \left(BR^{B-1}/R_o^B \right) \exp\left[-(R/R_o)^B \right] dR \quad , \qquad (1)$$

where R_o and B are constants for a given experiment, and the parameters for varied experiments. The equation is readily integrable, yielding for the fraction, F(R), of fragments of dimension greater than R, the expression:

$$F(R) = \exp\left[-(R/R_o)^B \right] \quad . \qquad (2)$$

The principal virtue of Eq. (2) is that, in most instances, it provides a reasonable fit to the data. The formulation has some vague theoretical justification for B = 1 in the one-dimensional case. A particular disadvantage of the expression is that the "constants" (especially B, which is primarily a "fudge" factor) may not be in any simple way related to the physical situation, so that their variation with changing experimental configurations may not be reasonably predicted.

J. N. Fritz of LASL Group GMX-6 has performed a theoretical investigation to determine a better based fragment distribution function.[4] In his work it was assumed only that the probability of occurrence of a separation plane was the same throughout the

4. J. Fritz, Appendix B, this report.

object to be broken. The expression he obtained bears some resemblance to Eq. (2) but, since Dr. Fritz did not permit himself the luxury of a second parameter, it does not provide a very good fit to the data of this work. From a comparison of his formulation with that of Rosin's Law, it is observed that an $\exp(-R/R_o)$ should be the dominant factor in any reasonably based distribution function, and that the parameter R_o should resemble, or be proportional to, the expected distance between breaks.

III. EXPERIMENTS AND ANALYSIS

The data discussed in this report are taken from 45 recovery shots fired on various graphite configurations. Eight of these shots were on approximately 1/3-scale models, and the remainder on systems ranging from 1/9 to 1/10 of full size.[5]

Four of the shots on larger-scale models were of a "dispersal-recovery" type. For these, the shots were fired in the middle of an open area, and the fragments were recovered on a sampling basis on large tarpaulins spread out over distances up to 500 ft. The shots were additionally instrumented with a Fastax camera and fiberboard screens at varying distances, upon which the amount of perforation was observed. A discussion of the dispersal is presented in Appendix A. The recovery information was regarded as rather untrustworthy for these experiments, as

5. For this investigation the reactor core, including the graphite outer cylinder, was taken as being a right circular cylinder 54 inches long by 40 inches diameter, and having a graphite weight of 1700 kg.

it was virtually impossible to obtain a "fair share" of the smaller pieces. The dispersal-recovery series included an experiment which represented the closest model to an actual Rover reactor. This arrangement, which incorporated actual B-1 elements and modules, is shown schematically in Fig. 1 and pictured in various stages of assembly in Fig. 2.

All of the other shots were performed with a 4 ft x 4 ft x 4 ft steel-walled recovery pit. The 1/3-scale models were fired suspended above the pit, as shown in Fig. 3, so that a certain segment of the cylindrical assembly was recovered. The smaller-scale models, such as are shown in Figs. 4 and 5, were fired inside the pit, approximately a foot from the bottom.

Two experimental problems were attendant to the recovery shots. The first was secondary breakage of the fragments upon striking the recovery chamber walls. This could have led to a determination of fragment size distribution which was too low, and probably selectively too low, since the larger pieces suffered less deceleration from air resistance, and reached the walls with higher velocity. Enough shots were fired to demonstrate that serious secondary breakage resulted if the pit walls were not lined with some soft material, and that a 1/4 in. neoprene rubber lining served as a

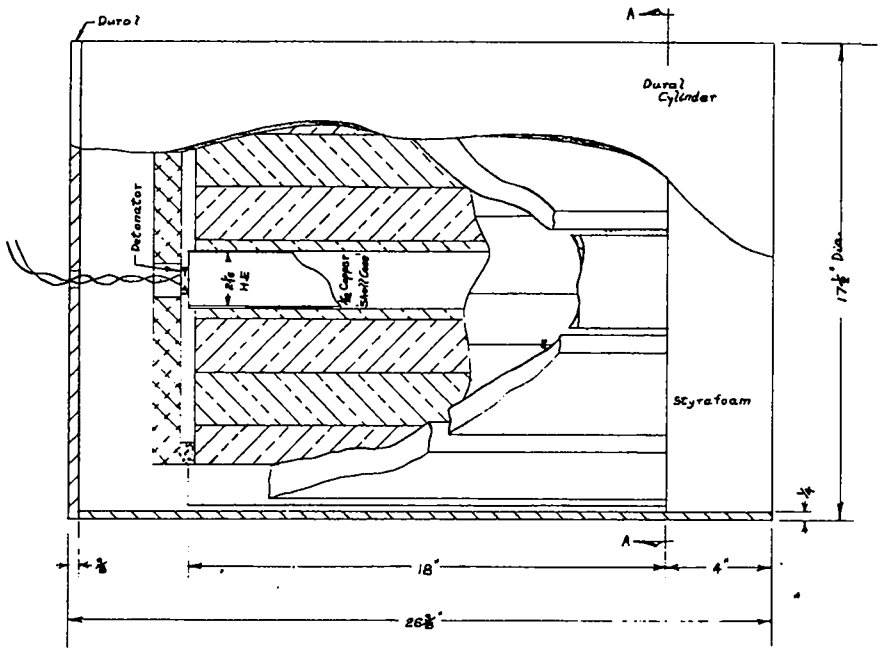

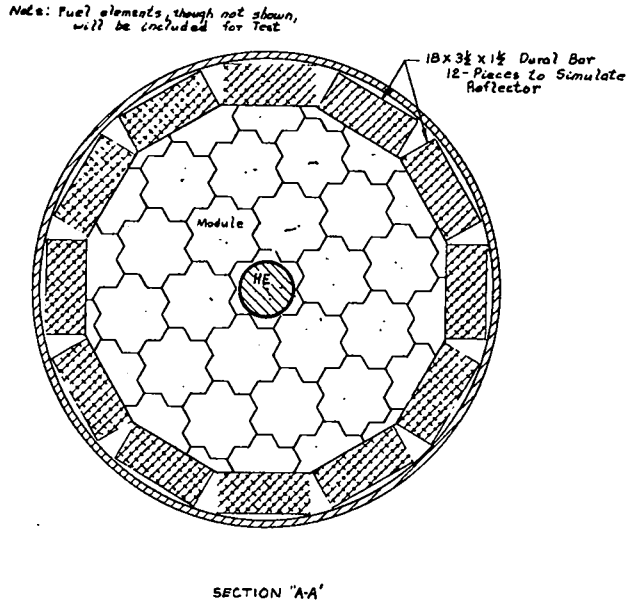

Fig. 1 Schematic drawing of 1/3-scale modular assembly. The modules employed were reject items from a B-1A assembly, and since they were full size, the model was not scaled in detail.

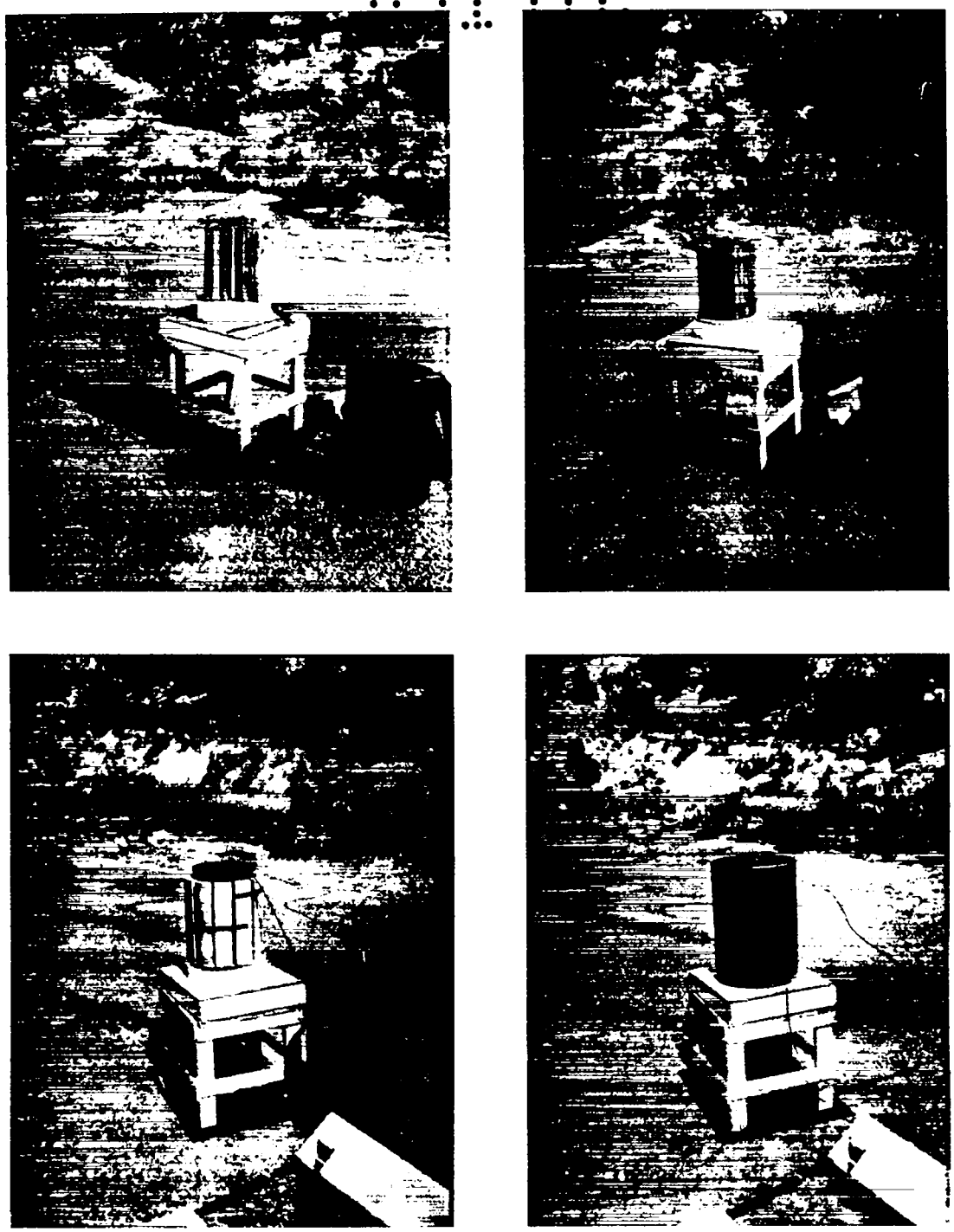

Fig. 2 Stages in the assembly of the modular model for dispersal-recovery shot RFS-6.

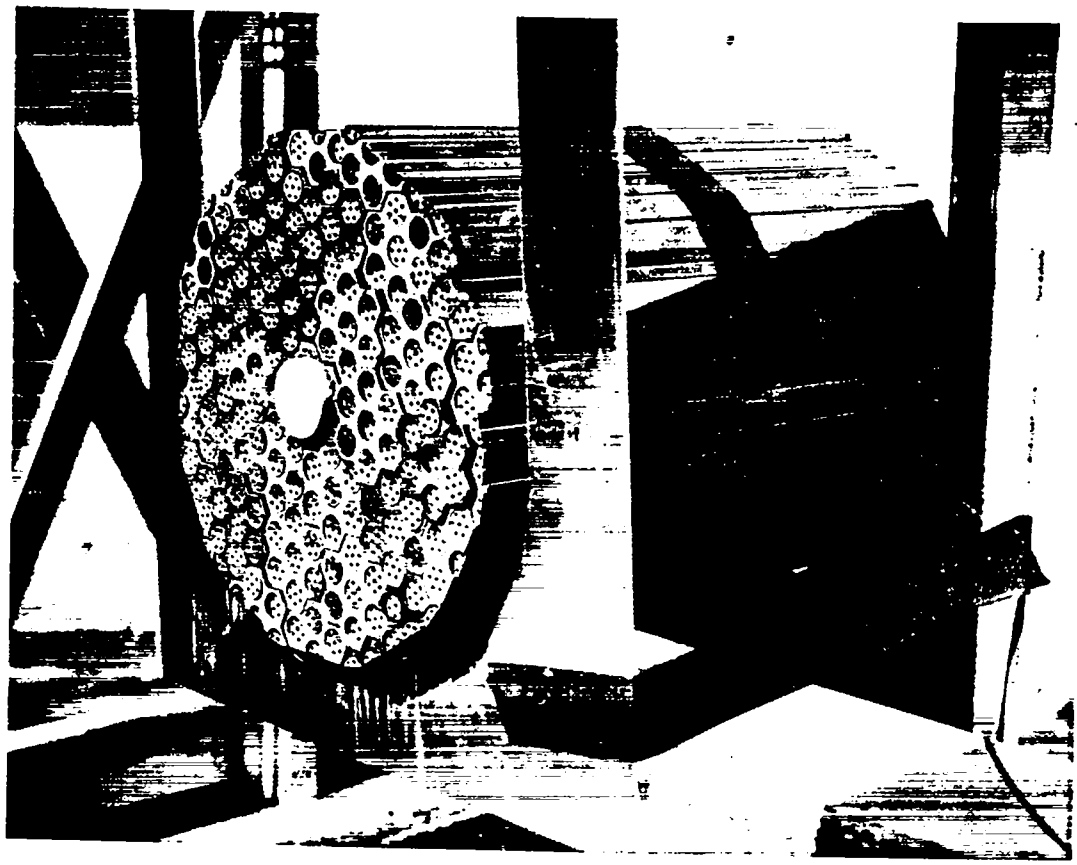

Fig. 3 Arrangement for 1/3-scale recovery shot. The shot shown is RFS-10, employing the same type of modular assembly as RFS-6, without the surrounding metal parts. The support mechanism was successful in reducing the amount of extraneous debris, such as wood splinters mixed with graphite, in the pit. The height chosen was scaled so the shot-pit floor distance was just 3 times the wall distance of the 1/9-scale shots, and resulted in an expected recovery of 1/4 the original mass of the graphite.

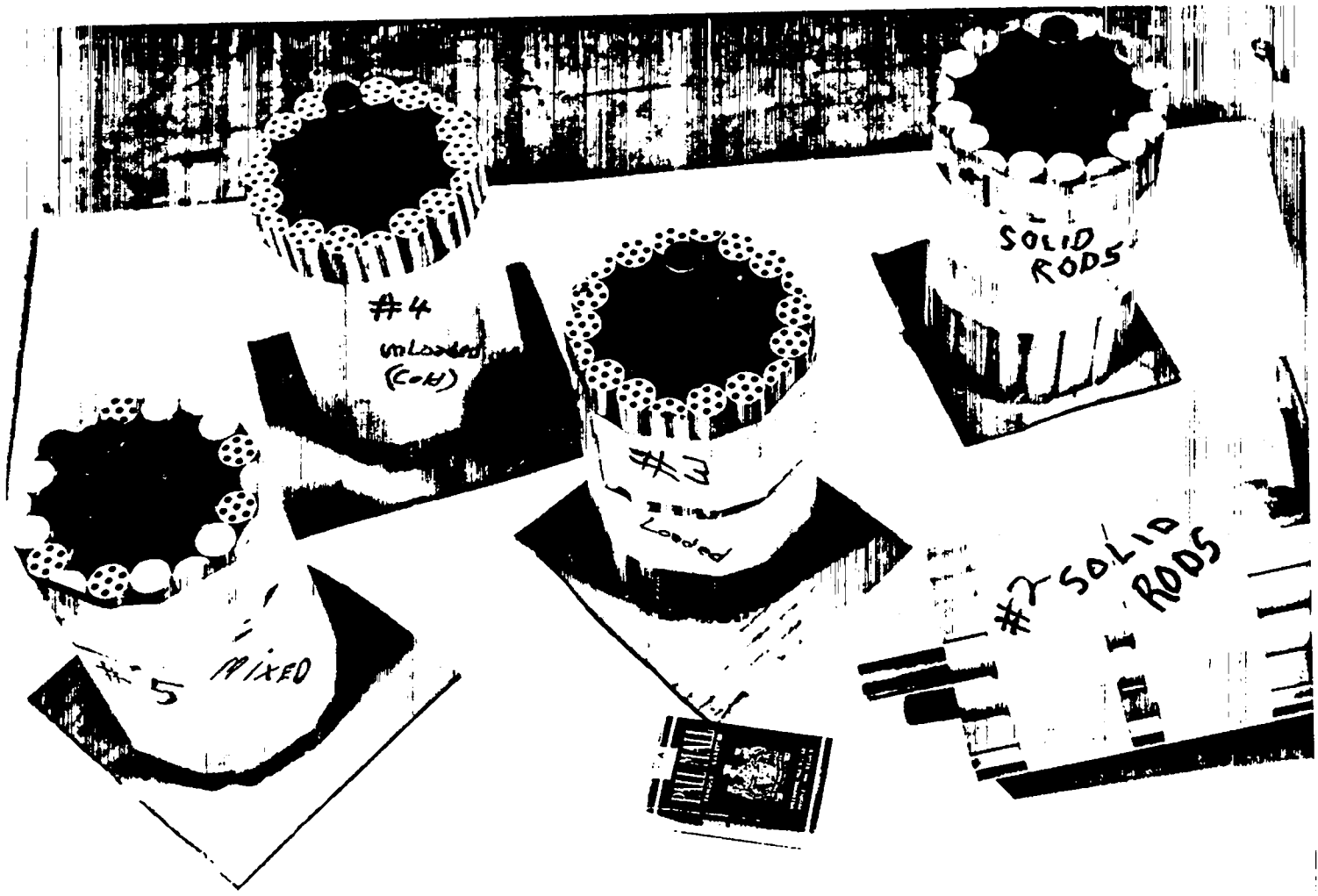

Fig. 4 Typical 1/9-scale rod and element configurations. The assemblies, commonly called "33-rod" shots actually consisted of 36 pieces, of which six were split lengthwise. Both the solid rods and the B-1A elements employed in these assemblies were 3/4" in diameter. The numbers shown correspond to the shot numbers listed in Table II in the R-series. Before firing, the 3/4" copper tubing was withdrawn from the assemblies and replaced with an explosive charge of the same diameter.

APPROVED FOR PUBLIC RELEASE

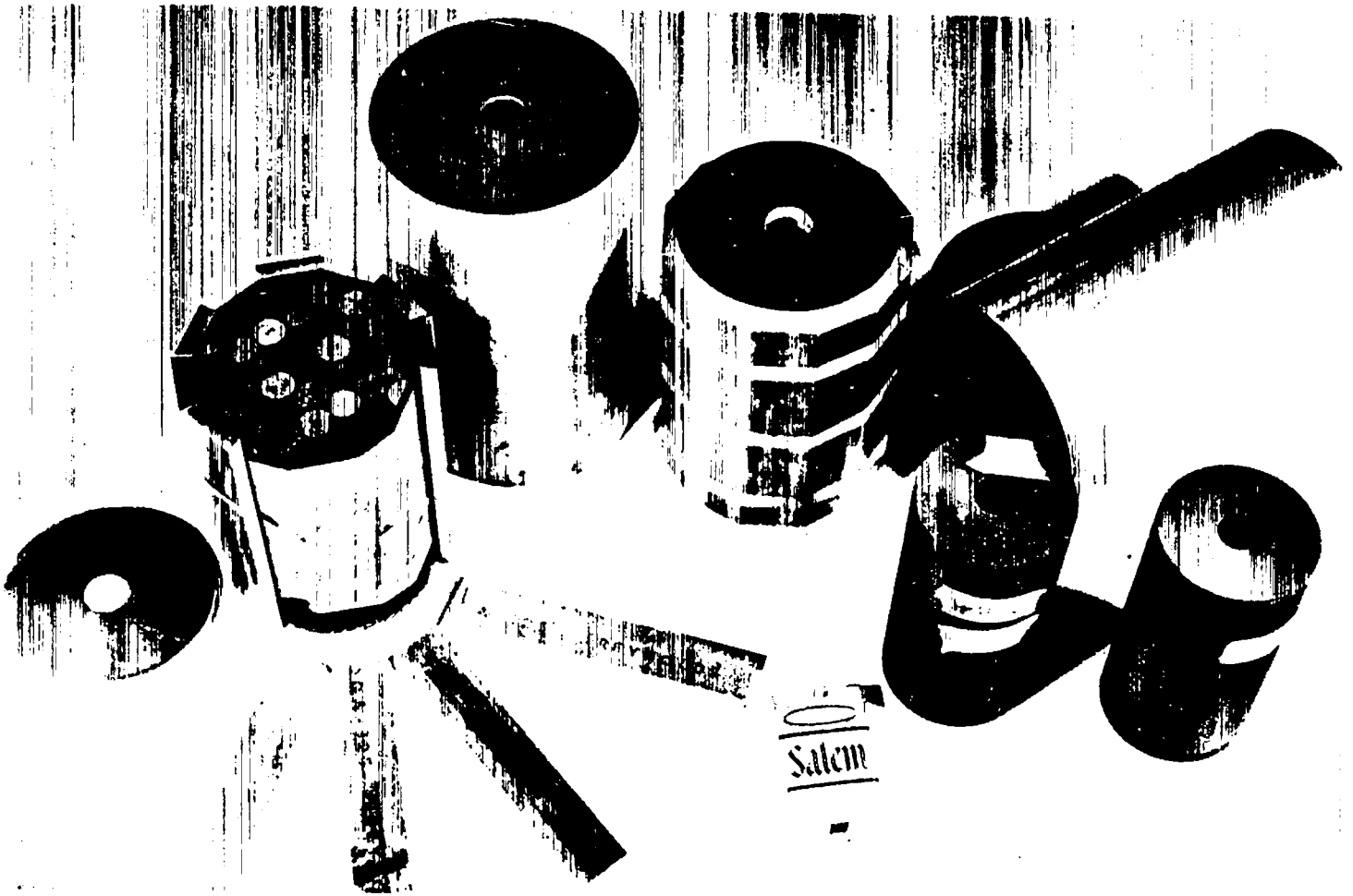

Fig. 5 Other 1/9- and 1/10-scale assemblies. As with the 1/3-scale configurations, the case mock-ups shown employed twelve Duralumin bars to inertially represent the beryllium reflector.

practical means of reducing the effect to an acceptable level.

The second problem was in estimating the size distribution of the fragments (approximately 15%) which were not recovered as expected. One could take the view that these pieces had the same size distribution as those recovered, or, after observing motion pictures of the great amount of smoke arising from a shot, assume that the entire loss belonged in the smallest fragment-size category. Computations were made on the basis of both assumptions, with the eventual decision to choose the first one, since it usually provided a better fit to Rosin's Law and, if in error, at least erred in the direction of pessimism.

After recovery, the fragments were separated into four to seven size categories by passing them through graduated screens. In addition to a pan to retain the smallest particles, sieves with square holes of width 4.76, 2.00, 0.84, 0.50, 0.25 and 0.105 mm were employed. The screening was done with a mechanical shaker, and the time of the operation controlled so that the fragments from each shot received the same treatment. Measurements of the weights retained by various size screens provided the data for fitting Eq. (2).

It is perhaps well to point out what is meant by the "di-

mension," R, employed in this discussion. In principle, a fragment which will pass through a screen of size R_s need have only a width and depth to or less than that value, and could be substantially longer than R_s. Fragments of length two to three times R_s have indeed been observed in this work, but of course these always have dimensions in the other directions somewhat smaller than R_s. For this study, it will be assumed that the largest fragment passing a given size screen is a cube with edges of that particular size. Consequently, the screen may be considered to divide the fragments into categories of volume more than and less than R_s^3. Since the fragments have a variety of shapes, the sharp division is not of course the case. An examination of the fragments indicates that to the extent the assumption employed is erroneous, it errs conservatively, i.e., toward the implication that the fragments are larger than is actually the case.

The data were fit to Rosin's distribution by least squares. To accomplish this, Eq. (2) was reduced to the linear form:

$$Y(R) = A - BX, \tag{3}$$

where

$$Y(R) = -\ln\left[-\ln F(R)\right], \tag{4-a}$$

$$X = \ln R, \tag{4-b}$$

$$A = B \ln R_o, \tag{4-c}$$

and B is the same as previously defined. The actual arithmetic was performed with an IBM-7090 computer.

When the data are presented graphically in this report, the result is usually in the form of Eq. (3). An examination of the expressions shows that R_o, corresponding to the value of R when Y(R) = 0, may be regarded as a "characteristic dimension"; in fact, the distribution indicates that a fraction, 1/e, of the fragments have dimensions larger than R_o. One may equally well define the values of R corresponding to other fixed fractions, such as $R_{0.01}$ and $R_{0.10}$ which are employed to indicate those dimensions dividing off, respectively, the largest 1% and 10% of the distribution.

Table I lists the graphite configurations for the 45 experiments and contains an explanation of the symbols employed in tables and text. Table II lists the initial conditions for the 45 experiments, along with the values of B and R_o. The standard deviation values listed for B and R_o, which are seen to vary from 2% to 10%, reflect how well the measured distributions fit Rosin's Law, and do not represent any estimate of the experimental error for the particular shot.

[redacted]
SIFIED

TABLE I. GRAPHITE CONFIGURATIONS AND OTHER SHOT NOTATIONS

A. Graphite configurations

1. Shots RFS-3, RFS-7, RFS-4, and RFS-5 were 12 in. diam by 18 in. long solid cylinders, with a 2-1/8 in. diam hole extending the entire length of the axis.

2. Shots RFS-8 and RFS-9 were "33-rod" assemblies consisting of 30 rods 2 in. diam by 18 in. long plus 6 half rods, arranged in a circular hexagonal close-packed array.

3. Shots RFS-6 and RFS-10 were fabricated of Kiwi B-1A modules and elements as shown in Figs. 1 and 2. The letter E refers to the fuel element portion of these assemblies, and M to the module portion.

4. All R-series shots except R-7 and R-8 were "33-rod" arrays as shown in Fig. 4.

5. Shot R-7 was a circular hexagonal-close-packed array of 132 3/8 in. diam rods, and R-8 was an array of 297 1/4 in. rods.

6. Shot HR-1 was a "33-rod" array of 7 in. long, hexagonal Kiwi B-4 fuel elements.

7. All S-series shots and shot G-1 were 4 in. diam by 7 in. long solid cylinders, with a 7/8 in. diam hole extending the length of the center axis.

8. All T-series shots were 3-1/2 in. diam by 7 in. long solid cylinders, with an axial 7/8 in. diam hole.

9. All W-series shots were 3-1/4 in. diam by 7 in. long solid cylinders, with an axial 7/8 in. diam hole.

SIFIED
[redacted]

B. Notations

1. Recovery type:

   R refers to shots fired completely within the 4 ft x 4 ft x 4 ft steel recovery chamber open on the upper face; the chamber itself was completely lined with 1/4 in. neoprene with an additional 1/8 in. layer of regions where the bulk of fragments impacted.

   R' refers to shots fired just outside the mouth of the recovery chamber lined with neoprene as above.

   S refers to a shot fired within the unlined recovery chamber in which the reactor mock-up was covered with a one-inch layer of Styrofoam.

   S' refers to shots fired just outside the mouth of the recovery chamber in which the chamber was completely lined with three to eight inches of Styrofoam. The thicker layer was at the bottom of the chamber, opposite the mouth.

   W refers to a shot fired in the unlined recovery chamber in which the reactor mock-up was covered with a four-inch layer of water.

   D refers to shots fired with the dispersal-recovery technique described in Appendix A.

2. Graphite type: A refers to AUC graphite, CS to CS-312 graphite, G to Graph-i-tite G, UE to Los Alamos unloaded fuel element material, LE to normal-loaded (0.4 gm depleted uranium per cm^3) Los Alamos graphite, and LEC to this material after a carbiding process. Further description appears in Section IV-D.

3. Cased: X indicates that Duralumin mock-ups of the pressure shell and reflector were used.

4. Explosive type: B refers to Composition B, C to Composition C and P to plastic bonded explosive, all further described in Section IV-B.

5. Explosive cased: X denotes that the charge was surrounded by 1/32 in. wall copper tubing, and XP denotes additional plastic filter between the explosive and the copper tube.

6. Explosive full scale equivalent: Equivalent weight, in pounds, in full-scale device having 1700 kg graphite.

7. Fraction original mass recovered: Values denoted by an asterisk were fractions of computed recovery expected from geometry of recovery system.

TABLE II. ASSEMBLIES AND COMPUTED ROSIN'S LAW PARAMETERS FOR RECOVERY SHOT PROGRAM

Detailed descriptions of graphite configurations, which are keyed to shot number designations, and explanations of other symbols are given in Table I.

Shot No.	Recovery Type	GRAPHITE DESCRIPTION Type	Cased	Weight (kg)	EXPLOSIVE DESCRIPTION Type	Cased	Weight (gm)	Full-scale Equiv. Weight(lb)	RECOVERY DATA Fraction Orig. Mass Recovered	B	Std Dev. B	R_o (mm)	Std Dev. R_o(mm)
1/3 Scale Solid Cylinders													
RFS-3	S'	CS		58.3	B	X	1679.0	108	0.81*	0.88	0.03	3.72	0.30
RFS-7	S'	CS		58.1	C	XP	879.0	57	0.86*	1.05	0.07	6.78	1.36
RFS-4	D	H4LM		60.8	B	X	1755.0	108	~ 0.8	1.28	0.06	5.48	0.70
RFS-5	D	CS	X	58.1	B	X	1693.0	109	~ 0.8	0.93	0.04	6.66	0.87
1/3 Scale Rod or Module Assemblies													
RFS-8	R'	A		53.6	B		1680.0	117	0.99*	0.62	0.03	1.53	0.15
RFS-9	R'	A		53.6	C	XP	635.0	44	0.92*	0.68	0.02	4.33	0.31
RFS-6	D	G+LE	X	68.2	B	X	1696.0	93	~ 0.8*	1.04	0.04	4.48	0.46
RFS-6E	D	LE	X	36.4	B	X	1696.0	93	~ 0.8*	1.10	0.09	2.57	0.46
RFS-6M	D	G	X	31.8	B	X	1696.0	93	~ 0.8*	1.14	0.03	6.88	0.47
RFS-10	R'	G+LE		68.2	B		1680.0	92	0.76*	0.70	0.04	1.30	0.12
RFS-10E	R'	LE		36.4	B		1680.0	92	0.76*	0.67	0.08	0.77	0.07
RFS-10M	R'	G		31.8	B		1680.0	92	0.76*	0.68	0.04	2.19	0.21
1/9 Scale Rod or Element Assemblies													
R-1	R	A		2.76	B		87.3	118	0.86	0.57	0.02	0.73	0.02
R-12	R	A		2.72	B		87.3	120	0.83	0.64	0.02	0.88	0.03
R-2	R	A		2.76	P		92.5	125	0.85	0.76	0.04	0.79	0.05
R-6	R	A		2.74	C	XP	40.0	55	0.98	0.55	0.04	2.52	0.43
R-13	R	A	X	2.77	B		87.3	118	0.88	0.62	0.01	1.88	0.08
R-7	R	A		2.82	B		87.4	116	0.97	0.66	0.02	1.10	0.04
R-8	R	A		3.16	B		87.2	103	0.72	0.68	0.03	1.06	0.06
R-3	R	LE		2.68	B		87.3	122	0.81	0.85	0.14	0.37	0.02
R-9	R	LE		2.69	C	X	60.0	84	0.62	0.68	0.04	0.73	0.04
R-11	R	LEC		2.68	C	X	60.0	84	0.84	0.75	0.05	0.87	0.06
R-4	R	UE		2.65	B		87.3	123	0.86	0.70	0.03	0.70	0.03
R-10	R	UE		2.66	C	X	60.0	84	0.83	0.75	0.03	1.10	0.07
R-5	R	A+LE		2.74	B		87.3	119	0.80	0.63	0.05	0.64	0.04
R-5E	R	LE		1.00	B		87.3	119	0.80	0.52	0.01	0.20	0.01
R-5R	R	A		1.74	B		87.3	119	0.80	0.61	0.01	0.98	0.01
HR-1	R	LE		2.79	B		87.3	118	0.77	0.61	0.03	0.52	0.02
1/9 Scale Solid Cylinders													
S-2	W	CS		2.40	B		87.3	136	0.55	1.30	0.07	0.85	0.05
S-4	S	CS		2.39	B		87.3	136	0.64	1.17	0.05	1.09	0.06
S-5	R	CS		2.38	B		87.3	137	0.86	1.04	0.02	1.01	0.02
S-6	R	CS	X	2.35	B		87.3	139	0.95	1.00	0.03	1.39	0.07
G-1	R	G		2.58	B		87.3	126	0.91	1.01	0.03	1.04	0.05

1/10 Scale Solid Cylinders

T-1	R	A		1.74	B		87.3	188	0.87	0.93	0.06	0.63	0.04
T-2	R	A		1.77	P		92.5	195	0.85	0.86	0.03	0.54	0.01
T-4	R	A		1.74	B	X	87.4	188	0.83	0.96	0.04	0.54	0.01
T-5	R	A		1.70	C	X	85.0	187	0.85	0.88	0.03	0.51	0.01
T-6	R	A		1.74	C	XP	43.0	93	0.88	0.95	0.02	1.23	0.05
T-7	R	A		1.74	C	XP	21.0	45	0.95	0.97	0.04	5.16	0.69
T-8	R	A		1.78	C	XP	21.0	44	0.97	0.91	0.05	6.20	1.03
T-3	R	CS		1.80	B		87.3	182	0.89	1.07	0.02	0.72	0.02
T-10	R	CS		1.81	P		92.5	192	0.86	1.08	0.02	0.69	0.01
T-11	R	CS		1.82	C	XP	21.0	65	0.96	1.01	0.03	5.19	0.45
T-9	R	A	X	1.74	C	XP	37.0	80	0.86	0.94	0.04	2.03	0.18
T-12	R	CS	X	1.81	B		87.3	180	0.87	1.02	0.04	0.94	0.05
W-1	R	A		1.65	C	X	85.0	193	0.69	0.95	0.06	0.41	0.01
W-2	R	A		1.54	C	XP	45.0	109	0.84	0.85	0.02	0.85	0.02
W-6	R	A		1.36	C	XP	21.0	58	0.85	0.88	0.02	1.96	0.07
W-4	R	G		1.64	C	X	85.0	194	0.88	0.99	0.02	0.49	0.01
W-5	R	G		1.66	C	XP	45.0	101	0.90	1.05	0.03	1.02	0.03
W-3	R	G		1.77	C	XP	21.0	44	0.98	0.97	0.03	3.81	0.03
W-7	R	G		1.67	C	XP	85.0	191	0.88	0.96	0.05	0.50	0.01

[redacted]

IV. COMPARISON OF CERTAIN FACTORS

A. Effect of Varying Explosive-to-Graphite Weight Ratios

This study has consistently shown that the parameter B is relatively unaffected by the explosive-to-graphite weight ratio, whereas increasing the relative amount of high explosive results in a corresponding reduction of the value of R_o. It in fact appears that, for a given type of graphite in a given geometry and dimension, the product of R_o and W_e (W_e is the ratio of the equivalent weight of high explosive to 100 lb) is roughly constant above a certain limit. The limits of the proportionality seem to be from about 60 lb full-scale equivalent weight of explosive to 200 lb. The products $R_o W_e$ are listed in Table III for certain sets of shots wherein other parameters were approximately the same.

As may be observed on certain small-scale shots (W-3, T-7, and T-8), the values of R_o are substantially larger than would be predicted by the proportionality. All of these shots involved 21 gm Composition C charges packed in Lucite tubes, with the

[redacted]

TABLE III. TESTS OF PROPORTIONALITY OF R_o AND EQUIVALENT EXPLOSIVE WEIGHT
(Both parameters are defined in text)

Shot No.	Configuration	W_e	$R_o W_e$ (mm)	$R_o W_e^{1.33}$ (mm)	$R_o W_e^{1.20}$ (mm)
RFS-3	Solid CS cylinder	1.08	4.02	4.12	4.09
RFS-7	12" diam x 18"	0.57	3.86	3.20	3.45
RFS-8	33 AUC rods	1.17	1.79	1.89	1.84
RFS-9	2" diam x 18"	0.44	1.90	1.45	1.62
W-1	Solid AUC cylinders	1.93	0.79	0.99	0.91
W-2	3-1/4" diam x 7"	1.09	0.93	0.95	0.94
W-6		0.58	1.14	0.94	1.02
W-4	Solid Graph-i-tite G	1.94	0.95	1.18	1.09
W-7	cylinders	1.91	0.96	1.19	1.09
W-5	3-1/4" diam x 7"	1.01	1.03	1.03	1.03
W-3		0.44	1.68	1.28	1.42
T-5	Solid AUC cylinders	1.87	0.95	1.17	1.10
T-6	3-1/2" diam x 7"	0.93	1.14	1.12	1.13
T-7		0.45	2.32	1.81	1.99
T-8		0.44	2.73	2.08	2.31
R-1	33 AUC rods	1.18	0.86	0.91	0.89
R-12	3/4" diam x 7"	1.20	1.06	1.12	1.10
R-6		0.55	1.39	1.13	1.23
R-3	33 loaded elements	1.22	0.45	0.48	0.47
R-9	3/4" diam x 7"	0.84	0.61	0.58	0.59
R-4	33 unloaded elements	1.23	0.86	0.92	0.90
R-10	3/4" diam x 7"	0.84	0.92	0.87	0.89

explosive dimensions 3/8 in. diam by 7 in. long. The density of packing was about the same as in other shots, and 3/8 in. is several times the failure diameter of Composition C. There is no obvious experimental reason for the failure of the proportionality rule in these smaller-scale shots, and it remains valid into the region of 50 lb equivalent high explosive in the 1/3-scale shot, RFS-7.

General trends in the data indicate, at least in the smaller-scale data, that R_o is slightly more strongly dependent on W_e than the straight inverse proportion. Consequently, a form of the type:

$$R_o \sim 1/W_e^k \qquad (5)$$

was computed for the various experiments, using k-values of 1.33 and 1.20. Examination of the two right-hand columns in Table III indicates that the use of the 1.20 value provides the best "rule of thumb" to fit the observations.

B. Effect of Explosive Type

Three types of high explosive were employed in this program:

1. Composition B (Comp B), a mixture of 60/40 by weight of RDX/TNT, in the form of machined castings of 1.72 gm/cm^3 density.

2. Composition C (Comp C), a plastic explosive composed primarily of RDX, hand-packed to a density between 1.3 and 1.4 gm/cm^3.

3. 9404 Plastic Bonded Explosive (PBX), consisting of 94% HMX explosive in a binder, with density of 1.825 gm/cm^3.

In the one pair of shots (T-4 and T-5) in which the comparative effects of Comp B and Comp C could be observed, no significant difference in fragmentation was noted. In three pairs of shots in which the effect of PBX could be compared with that of Comp B, it was found, after compensating for equivalent explosive weight, that in one the use of PBX reduced R_o by 11%, in another the change was less than 1%, and in the third the R_o value was 14% larger. Uncontrolled factors and lack of reproducibility have a greater effect than does changing from one to another of these rather similar explosives. In future computations, no compensation will be made for whichever of these three types of explosive is used.

The three explosives employed in this study are actually quite similar in properties, composition, detonation pressure, and products. An explosive of a somewhat different type shows some possibilities for increased fragmentation of a reactor core.

Oxygen-rich high explosive diluted with aluminum (frequently called ALEX) has been recognized for some time as possessing some virtue as a bursting charge in large-scale blasting operations, and is presently favored for use in depth charges. Fickett[6] has computed that a mixture of 2 moles of aluminum with one of ammonium nitrate has a total available energy about 55% greater than RDX. However, the aluminized explosive releases its energy substantially later in the detonation process than do explosives of the type employed in this work. The work done by an explosive depends upon the degree to which the product gases are allowed to expand; and aluminized explosives require substantially more expansion, or less confining pressure, to liberate their chemical energy than do more conventional types. The question reduces to this: at what confining pressure is the fragmentation of the graphite concluded. The detonation pressure, and consequently the initial stress introduced into the core configuration, is actually less for the NH_4NO_3-Al mixture than for RDX. According to Fickett's calculations, the aluminized material would not exceed the RDX in energy release until the explosive had relieved to around 15 kb

6. Wildon Fickett, Private Communication. (March, 1962).

pressure. At 1 kb the aluminized material provides only about 11% more work than the RDX, at 0.1 kb about 19% more, and only 31% more at atmospheric pressure. If one considers that shock-induced fracture, the principal mechanism by which the graphite is broken, requires pressures of the order of 100 atm, the gain from the use of aluminized explosives does not appear substantial. It is possible that the degree of fragmentation depends entirely on the strength of the initial shock, in which case the aluminized explosive would prove inferior. However, it is also possible that some of the fragmentation is accomplished through abrasion by escaping detonation products, in which case the presence of aluminum could serve to enhance the reduction of the core.

C. Effect of Change of Scale

One pair of shots in the program provides a reasonable comparison of the fragmentation of solid cylinders of substantially different sizes. If the fragment distributions from shots RFS-3 (1/3-scale CS-312 graphite cylinder) and S-5 (1/9-scale cylinder of the same material) are compared, it is seen that the values of B do not differ substantially, and that the figures for R_o differ by roughly a factor of three. More precisely, the ratio of the cube

root of the graphite volumes for the two shots is 2.86, and that for the values of $R_o W_e^{1.20}$ (which corrects for difference in explosive equivalent weight) is 2.78. The implied scaling rule is that the fragment distribution should have a characteristic dimension, R_o, directly proportional to the original dimensions (as manifested by the cube root of the volume) of the assembly.

Two available comparisons of 1/3- and 1/9-scale AUC rod configurations do not quite bear out the above rule. The ratio of original dimensions for these comparisons is 2.63, whereas the ratios of $R_o W_e^{1.20}$ are 2.07 (RFS-8 vs R-1) and 1.32 (RFS-9 vs R-6). Though these comparisons do not especially well demonstrate the form, in this work the rule

$$R_o W_e \sim (\text{Original graphite volume})^{1/3} \qquad (6)$$

will be employed for configurations of identical geometry and material, with the usual consideration that the error is conservative.

Such a scaling rule is equivalent to a detailed application of the similarity principle. This principle, as expounded by Cole,[7] asserts that the pressure and other properties of a shock

7. Robert H. Cole, Chap. IV Underwater Explosions, Princeton University Press (1948).

process remain unchanged if the scales of time and length by which they are measured are altered by the same factor as are the dimensions of the explosive charge. To extend the principle to this problem, one may argue that a "break" occurs at a given point in a graphite assembly when a certain limiting strain is reached at that point, and that the fragment size distribution is dictated by the spacing of these breaking points. Thus, if the size of an assembly is tripled, the explosion results in exactly the same values for the shock-wave parameters in a space and time scaled by a factor of three, with the breaking points occurring three times as far apart and the recovered pieces being three times as large as those from the smaller experiment.

The principle of similarity argued above always requires that the process be nondissipative, i.e., that the medium in which it occurs be hydrodynamically ideal. Graphite, far from having this feature, displays an anomalous compressibility at lower pressures, so that normal steep shock fronts are not developed. It appears that this property could explain the fact that the rod assemblies fail to "scale" in the manner of the solid cylinders.

The scaling rule stated above, and this study, are in

[redacted]

contradiction to an approach attempted earlier in the program. In the previous concept, it was proposed that in a given geometrical configuration, regardless of scale, the efficiency of the explosive energy in producing surface area would remain constant. The energy required to produce unit surface area was assumed to be that required to vaporize one layer of atoms from it. Thus, regardless of scale, the surface generated per unit volume would be the same, and with any reasonable description of the fragment-size distribution (i.e., one not employing the second parameter, B), the size of the pieces recovered would prove independent of the size of the original assembly. As well as being inconsistent with the scaling observations, this approach allows for little sensitivity in fragment size as a function of mechanical yield strength of the material. It will be shown in Section D that mechanical yield values do sometimes influence the fragmentation of the graphite.

D. Effect of Physical and Mechanical Properties

After the early dispersal-recovery shot on the modular B-1A mock-up (RFS-6), the fragments were separated with a high density liquid into two classes. One class included those fragments originating from the Graph-i-tite G modules, and

[redacted]

the other those originally part of the normal-loaded (i.e., containing 0.4 gm/cm^3 depleted uranium) elements. The fragment distribution for the loaded material was found to tend toward smaller sizes than the one for Graph-i-tite G. This implied that either the physical properties or the geometry, or both, of the original materials strongly influenced the fragmentation of the graphite.

To eliminate the effect of the geometry, two identical configurations were fired at 1/9-scale, one of which (R-3) employed normal-loaded graphite elements, and the other (R-4) "unloaded elements." These last were rods of the same shape as the loaded elements, produced by a similar method from similar carbon material. As seen in Fig. 6, the loaded material produced substantially smaller fragments.

In shot R-5, an assembly of 3/4 in. diam AUC rods combined with normal-loaded fuel elements (see Fig. 4) was fired. The distributions obtained are compared in Fig. 7 with corresponding "pure" AUC rod and fuel element shots in similar configuration. As is seen, mixing the two materials appears to increase the differences in their fragmentation; i.e., the more finely shattering fuel elements became still more finely divided

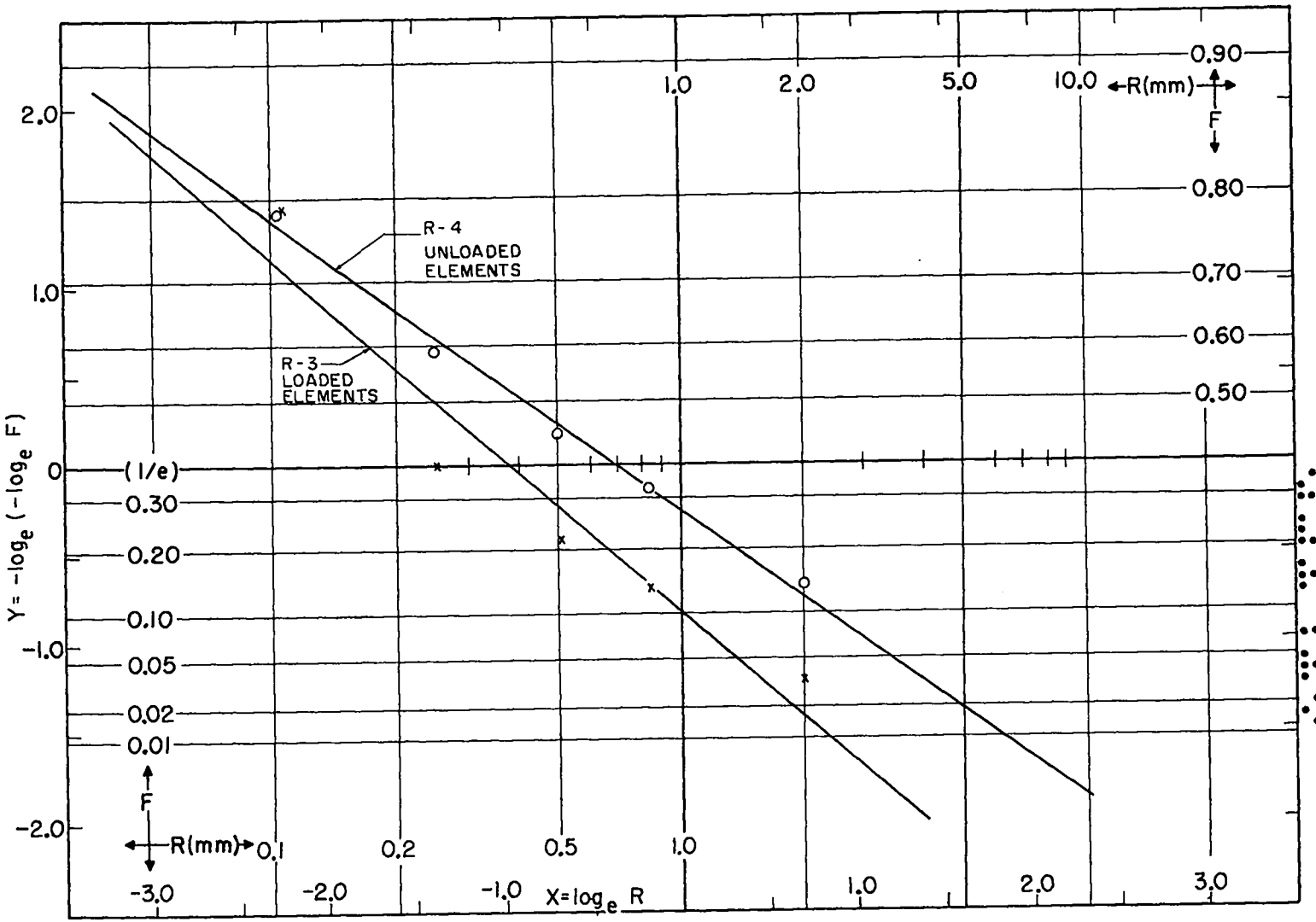

Fig. 6 Comparison of fragment distributions from similar experiments with normally-loaded and unloaded fuel element assemblies. The nature of the graphical representation employed is discussed at the end of Section III.

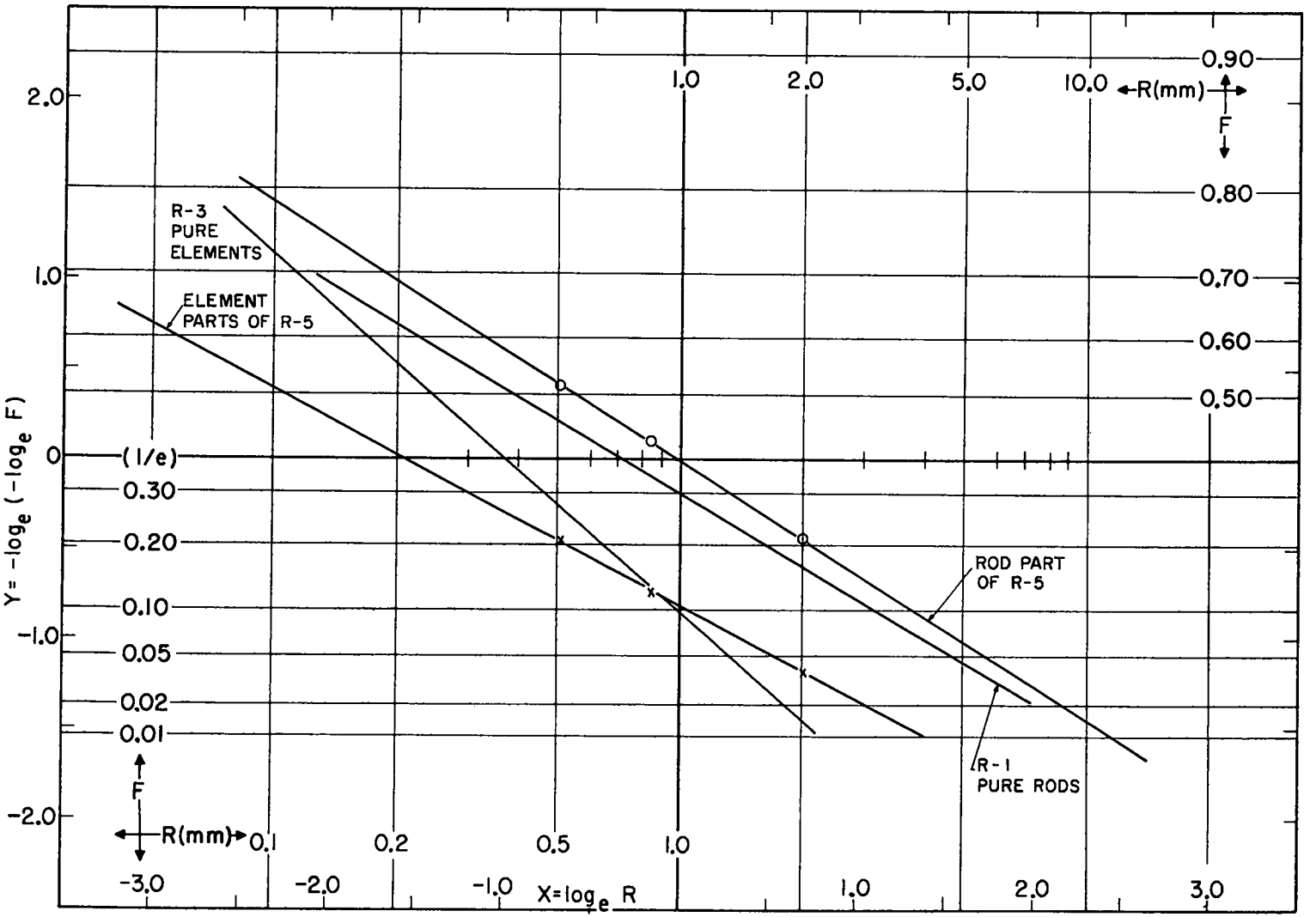

Fig. 7 Comparison of fragment distributions from normal-loaded element component and solid rod component of mixed 1/9-scale assembly.

in the mixed shot, and the coarser AUC portion became more coarse.

Experiments R-3 and R-4 clearly demonstrated that some property arising from the presence of uranium in the graphite increased the degree of fragmentation. One interesting, if unlikely, explanation of the effect is that some manner of inertial separation of the uranium and graphite under shock leads to the enhanced fragmentation of the loaded material. In work at Lawrence Radiation Laboratory, plastic loaded with finely divided lead has been observed under shock with framing cameras and flash x-ray, simultaneously. A definite separation of the lead component from the lighter plastic was seen.

Neglecting the above suggestion, the property of uranium-loaded graphite most likely to cause the smaller pieces is its greatly reduced mechanical strength. Studies in LASL's N-Division[8] have shown that most mechanical strength properties of the loaded material are reduced by a factor of two to four below those of its unloaded counterpart. The effect is especially pronounced when the loaded material (so-called "shelf-type") is aged in a normal

8. P. N. Wagner, and A. M. Gage, Private Communication.

atmosphere, in which case the observed weakening is associated with the conversion of 20 to 30% of the uranium carbide component to uranium oxide. To check the effect of this strength alteration, one assembly of fuel elements was "re-carbided" by heating in a furnace and kept in an inert atmosphere until fired. The fragment distribution from this assembly is compared in Fig. 8 with that of shelf-type loaded elements and unloaded elements. It is seen that the distribution for the carbided elements lies intermediate between those for the other two tests, indicating a definite increase in fragment size after the process. Since, in being run outside the atmosphere, the NERVA engine would also subject the fuel elements to this carbiding procedure, it seems that some degree of carbiding should be considered in an estimate for an actual destruct situation.

To further study the effect of physical properties on the fragmentation of graphite, the results from the shots on the three types of graphite (AUC, CS-312 and Graph-i-tite G) employed in solid cylinder configurations were compared. The information discussed in the previous sections was employed to correct for differences in explosive weight and scale.

If one applies the rules for scaling and equivalent explosive

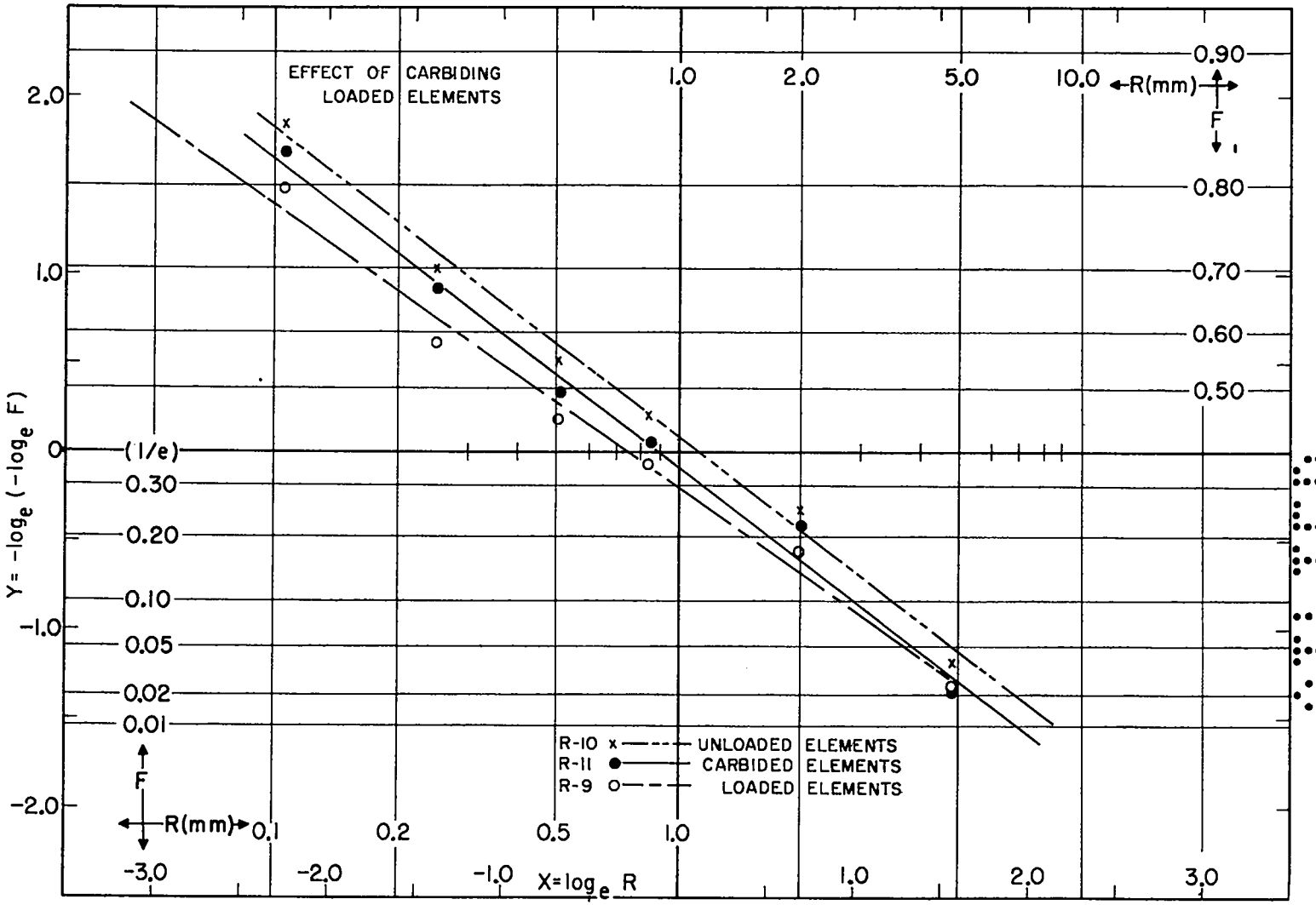

Fig. 8 Effect of the carbiding of normal-loaded elements on the fragment distribution obtained.

APPROVED FOR PUBLIC RELEASE

weight stated in previous sections, a "normalized characteristic dimension," R_n, may be written:

$$R_n = 100\, R_o W_e^{1.20} V_g^{-1/3} . \qquad (7)$$

W_e and R_o have been previously defined, V_g is the volume of graphite in cm^3, and the factor of 100 arises from considering the graphite volume of the full-scale engine to be 10^6 cm^3. If the choice of allowance for scale and explosive weight is correct, variations in R_n should be primarily due to differences in physical properties of the graphite and in the geometric configurations in which it is employed.

Table IV shows values of R_n for the shots on solid cylinders, excluding both those in which metal parts were employed and the 21 gm Comp C shots mentioned in Section IV-A. It is now seen that the average values obtained have hardly a significant, and certainly not a substantial, difference.

Data on the mechanical properties of graphite are scarce, and subject to wide variation among "identical" samples. A handbook value[9] for the tensile strength of CS-grade graphite is

9. Industrial Graphite Engineering Handbook, National Carbide Co., New York (1959).

[redacted]

TABLE IV. NORMALIZED CHARACTERISTIC DIMENSION ON SOLID CYLINDERS

Shot No.	Cylinder Diam (in.)	W_e	R_n (mm)	R_n (avg.) (mm)
	AUC Graphite			
T-1	3-1/2	1.88	13.3	
T-2	3-1/2	1.95	11.9	
T-4	3-1/2	1.88	11.4	
T-5	3-1/2	1.87	10.7	11.1 ± 0.8
T-6	3-1/2	0.93	11.2	
W-1	3-1/4	1.93	9.5	
W-2	3-1/4	1.09	9.9	
W-6	3-1/4	0.58	10.7	
	CS-312 Graphite			
T-3	3-1/2	1.82	14.6	
T-10	3-1/2	1.92	15.0	
S-5	4	1.37	13.3	13.3 ± 0.9
RFS-3	12	1.08	12.9	
RFS-7	12	0.57	10.9	
	Graph-i-tite G			
W-4	3-1/4	1.94	11.4	
W-5	3-1/4	1.01	10.8	11.5 ± 0.4
W-7	3-1/4	1.91	11.4	
G-1	4	1.26	12.5	

[redacted]

about 1400 psi. Morton Smith of LASL Group CMF-13 has made measurements on the other two materials employed as solid cylinders in the work.[10] He found room temperature tensile strengths ranging from 2400 to 4000 psi for Graph-i-tite G. The few samples of AUC graphite tested broke at the specimen thread, rather than the "neck," implying some type of notch sensitivity. The strength values obtained ranged from 2500 to 3000 psi. Thus, available figures yield the rather strange indication that the weakest graphite provides the distribution of largest fragments.

Barring such an unreasonable suggestion, other properties of the graphite must explain the differences and perhaps compensate for the anomalous correlation with tensile strengths. Two possible "other properties" are brittleness and grain size. A more brittle nature, as manifested by the notch sensitivity of the AUC material, could lead to enhanced fragmentation. The maximum grain sizes reported[9, 10] for CS, AUC and Graph-i-tite G materials are, respectively, 0.030, 0.008 and 0.003 in., with the larger grained material correlating to that producing the larger fragments.

10. Morton Smith, Private Communication.

In conclusion, the fragmentation distribution, R_n, must bear some relation to the physical and mechanical properties of the material; however, except for the shelf-type loaded material, the differences are small. There appears to be no simple method of correlation. The subsequent approach in this report will be to employ conservatively estimated values of R_n, based on the experiments available, as empirically characteristic of the material. As will be shown, R_n does not appear very sensitive to geometry.

E. Effect of Geometrical Configurations

It is unfortunate that while the geometrical configuration of the elements of a reactor engine could be the most dominant influence on its fragmentation with high explosive, obtaining acceptable data on this aspect was the most difficult part of the program. The difficulty arose from the unavailability of 1/3- or 1/9-scale pieces which could adequately detail the geometry of the actual engines. Thus, while some general rules may be derived to correlate to the small-scale shots on aggregates of rods and elements, the question as to whether they will apply at full scale remains.

One empirical observation, from examination of Table II,

is that the geometric configuration alone has a strong influence on the parameter B. Neglecting the dispersal-recovery data, it can be observed that fits to data obtained from assemblies involving aggregates of rods result in a set of B-values clustered around a figure of about 2/3, while those obtained for experiments on solid cylinders group around unity. The scatter in the values obtained is quite large, and the statement above may not be extended to a more detailed correlation to the particular type of geometric configuration, i.e., specific values for modular assemblies with elements, solid rod, aggregates, etc. However, the observation is consistent enough to give a value of B = 2/3 as a crude "rule of thumb" for rod configurations.

The values computed for R_n for 1/9-scale rod assemblies are shown in Table V. It may be noted that the values for AUC graphite average about 18% lower than those for the solid cylinders. While, with the accuracy of the experiments, this figure is considered hardly significant, it is assumed that the smaller values result from the geometry effect. It is further believed that, had it been possible to obtain unloaded element materials in rod form, the fragmentation from such assemblies would have produced an R_n value similar to that of AUC graphite. Thus the

[redacted]

TABLE V. COMPUTED PARAMETERS FOR RODS OF ELEMENT AGGREGATE SHOTS

Shot No.	B	R_n (mm)
Solid AUC Rods		
R-1	0.57	7.4
R-12	0.64	9.1
R-2	0.76	8.7
R-6	0.55	10.2
R-7	0.66	10.9
R-8	0.68	9.1
Normal-loaded B-1A Elements		
R-3	0.85	3.9
R-9	0.68	4.8
R-11	0.75	5.8
Unloaded B-1A Element Shape		
R-4	0.70	7.5
R-10	0.75	7.4
Normal-loaded B-4 Elements		
HR-1	0.61	5.2

[redacted]

20% lower value observed for the element shapes is considered primarily due to the seven holes in these assemblies. The further reduced values of R_n for the loaded elements resulted from the presence of uranium, discussed in the previous section. In the single experiment done, there was no significant difference between the hexagonal nineteen-hole B-4 elements and the B-1A elements. In the comparison of shots R-1 and R-12 on 3/4 in. AUC rods with R-7 on 3/8 in. rods and R-8 on 1/4 in. rods, it was hoped to obtain some feeling for the effect of reduced rod diameter. The shots were made with roughly the same volume of material, the same type of graphite, and the same fraction of voids in the hexagonal close-packed assemblies. The values of R_n were found to be slightly larger for the smaller rods, but after comparing the "identical" R-1 and R-12 it is difficult to attach much significance to the rather small difference.

To further allow for the effect of geometry, the form of the distribution law employed was modified to admit no fragments over a specified maximum dimension, R_{max}. The differential form of Rosin's Law, Eq. (1), was considered correct as R ranged from 0 to R_{max}, and it was assumed that (dF/dR) vanished for larger values of R. Thus, for the normalization involved for

Eq. (2), the integration of Eq. (1) was performed only to R_{max} rather than to infinity. The modified form thus obtained is:

$$F(R) = \frac{\exp\left[-(R/R'_o)^{B'}\right] - \exp\left[-(R_{max}/R'_o)^{B'}\right]}{1 - \exp\left[-(R_{max}/R'_o)^{B}\right]} \tag{8}$$

The parameters R'_o and B' are now slightly different from the similar quantities in the nontruncated expression, and R'_o does not, like R_o, represent the dimension dividing off a fraction, $1/e$, of the larger fragments.

Actual fitting of the data to Eq. (8) was accomplished on the computers by an iterative process. The least squares fit was made to the data initially in the nontruncated form; then new, fictional data points $F_i^{(j+1)}$ were defined:

$$\begin{aligned} F_i^{(j+1)} &= F_i^{(j)} + \exp\left[-(R_{max}/R_o^{(j)})^{B^{(j)}}\right](1 - F_i^{(j)}) \\ &= \exp\left[-(R/R'^{(j)}_o)^{B'^{(j)}}\right] \end{aligned} \tag{9}$$

and the least squares process repeated. In general, five iterations were employed, and in no case did the values of $B'^{(j)}$ and $R'^{(j)}_o$ alter as much as 1% between the last two iterations.

While it will be seen in the next section that the choice of R_{max} can strongly influence the estimates of particle size

distributions for the fragmentation of full-scale reactors, the selection did not seriously alter the fit over the range of screen sizes and the geometric configurations employed in this work. In general the value selected for R_{max} for aggregates of solid rods was the rod diameter. Keeping in mind that in this study the quantity R is identified with a volume R^3, the invariable observation on examining the larger fragments is that such a choice is quite large enough. The fit to the data of shot R-8, which involved 1/4 in. AUC rods, shown in Fig. 9. Two means of choosing R_{max} were employed for experiments with fuel element configurations. The first was to use the element diameter, and the second, to use a distance approximately equal to the separation of second-nearest neighbors in the hole array in the elements. The examination of recovered element pieces favors the second choice. In the great amount of fuel-element rubble accumulated in the program, a piece with an included hole was seen only in the exceptional case cited in Section VI. Figure 10 shows the fit to the data from shot HR-1, based on the two assumptions of R_{max}.

The values of R'_o and B' are shown in Table VI for those shots in which the application of a maximum fragment size made a significant change. Comparison with Table II shows that the

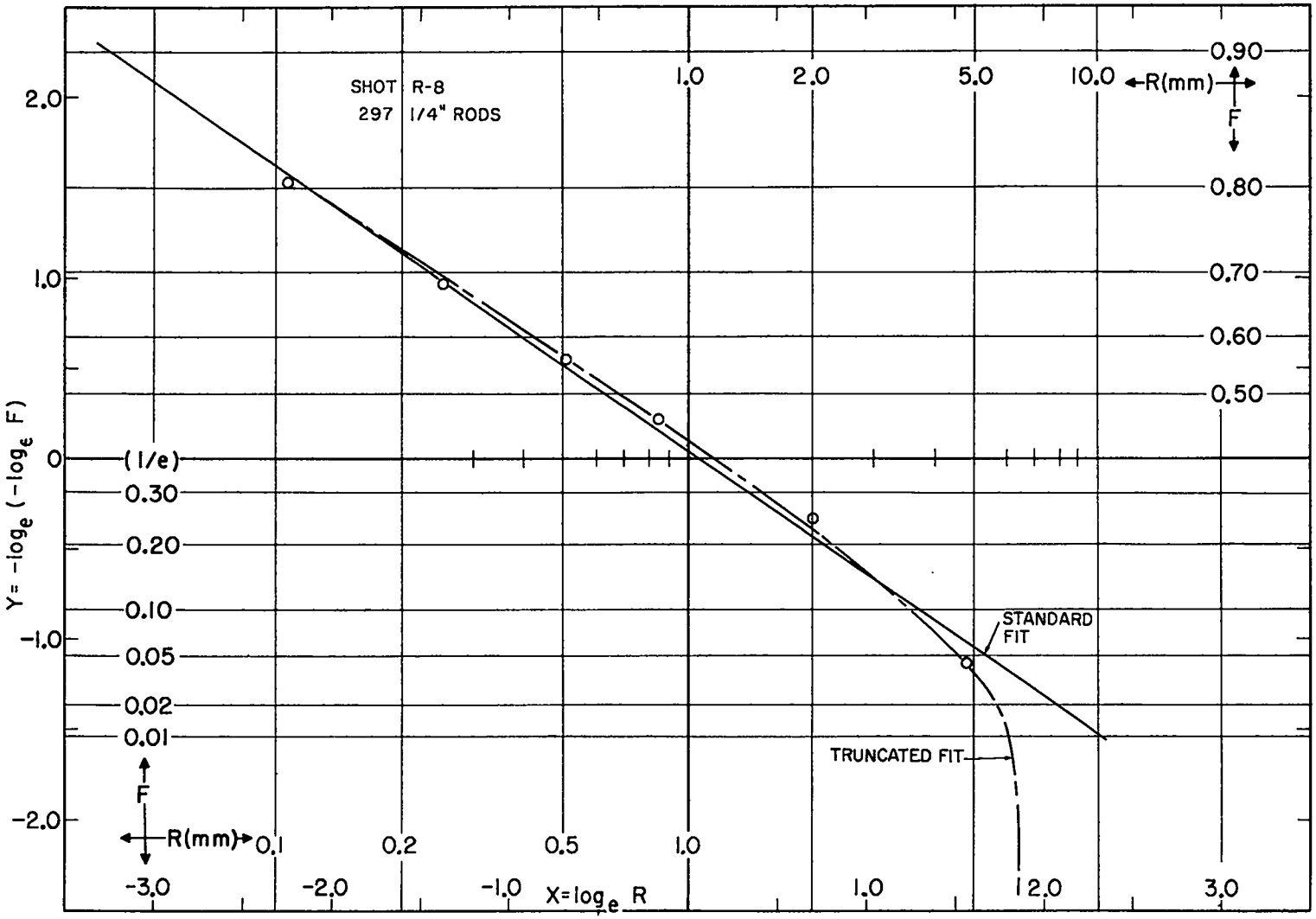

Fig. 9 Nontruncated and truncated Rosin's Law fits to experimental fragment distributions for shot R-8 on a 1/4 in. AUC rod assembly. The truncated distribution, of course, no longer represents a straight line in the coordinate system which has been used to represent the data.

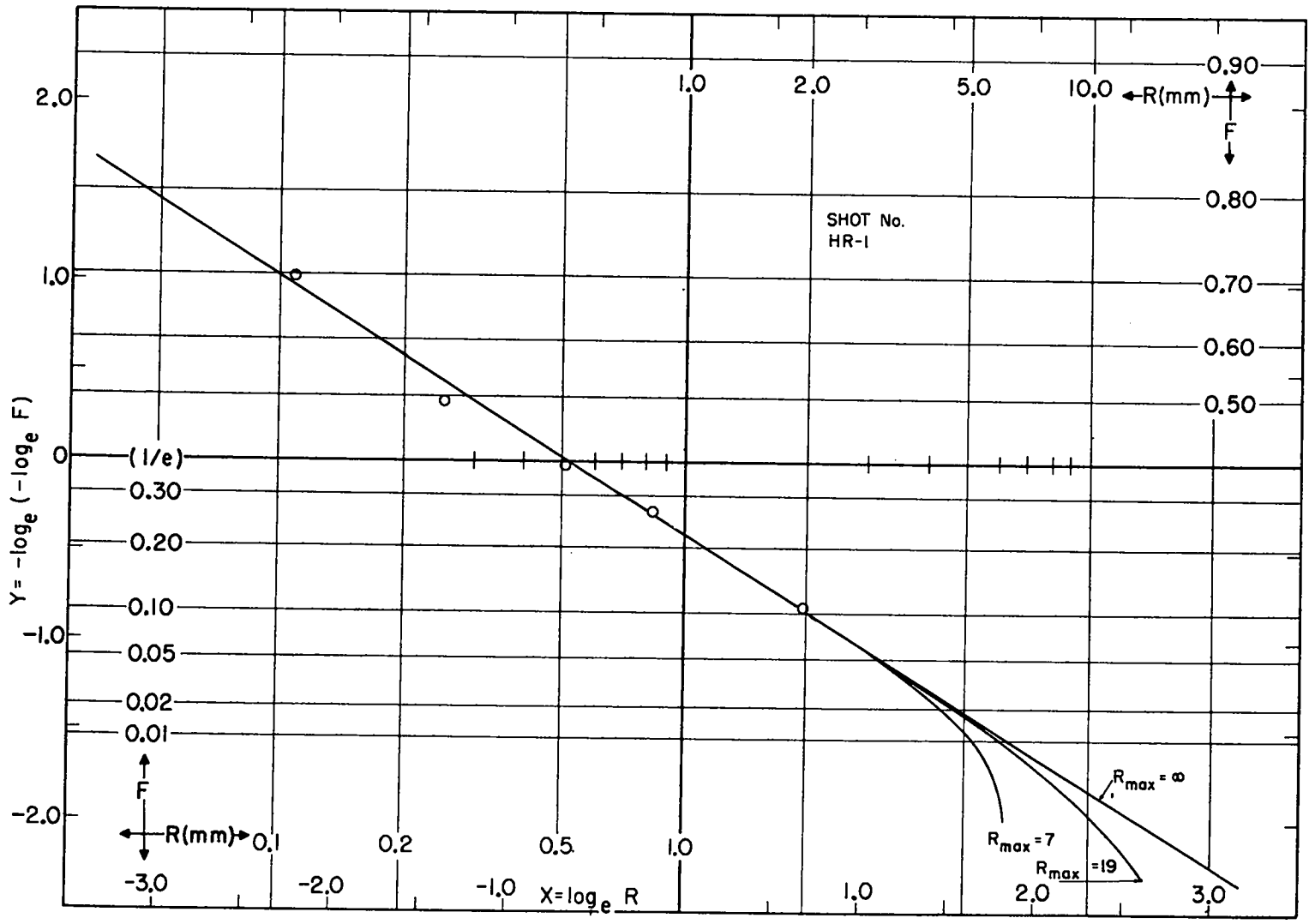

Fig. 10 Nontruncated fit to distribution data from a 1/9-scale element assembly and truncated fits assuming different values for R_{max}.

[redacted]

TABLE VI. COMPUTED PARAMETERS FOR TRUNCATED DISTRIBUTION

Shot No.	R_{max} (mm)	B'	R'_o (mm)	R'_n (mm)
AUC Rods				
R-6	19.0	0.53	3.37	13.6
R-7	9.5	0.64	1.21	12.0
R-8	6.4	0.62	1.41	11.9
R-13	19.0	0.62	2.00	20.0
RFS-9	50.8	0.68	4.38	5.0
Element Configurations				
R-10	19.0	0.75	1.11	7.5
R-10	11.0	0.75	1.12	7.6
R-4	11.0	0.69	0.71	7.6
R-9	11.0	0.69	0.74	4.9
R-11	11.0	0.75	0.87	5.8
HR-1	7.0	0.60	0.54	5.4

[redacted]

invariable result of truncating the distribution was an increased R_o and decreased B. The standard deviations of these parameters were altered little, and were worsened as often as improved. However, as a general rule, the fit to the data was improved for points corresponding to the larger mesh screens, which is of course the area of primary interest in the study.

In summarizing the geometry, it may be pointed out that there are two partially compensating hydrodynamic effects obtained in going from solid configurations to those involving aggregates of rods and holes. Certainly, the rod or element assemblies are more subject to fragmentation from a given shock strength, due to the many more sites for stress concentration and interactions of rarefactions. On the other hand, the numerous voids in the divided assemblies tend to attenuate the shock far more than does the continuous medium. Apparently in the configurations tested in this program, the first effect slightly dominates the second.

F. Effect of Metal Parts

A few shots were fired with simple inertial mock-ups of the beryllium reflector and the Duralumin pressure shell surrounding the graphite core model. These arrangements,

[redacted]

depicted in Figs. 1, 2 and 4, substituted Duralumin for the beryllium parts, since the two metals have approximately the same shock impedance.

The effect of the presence of the "cases" is considered in Table VII in terms of direct comparison of the values of R_n. It is seen that the case resulted in an increase in the value R_n of 21% to 42% for systems with solid cylinders, and in a factor of two increase in the one experiment with rod aggregates.

As with geometric variations, the presence of the metal parts about the graphite could be considered to have partially compensating hydrodynamic effects. The degree of breakup would be aided by the case to the extent that it confines the energy of the explosive and increases the time in which the product gases act upon the core. Conversely, most of the explosive energy is employed to provide kinetic energy for the surrounding material, and if more is required to accelerate metal parts, there is less left to shatter the core. Also the presence of material representing a fair impedance match about the graphite must result in some reduction of critical strains at the periphery of the core caused by the rarefaction waves and their interactions.

The indisputable evidence of the program is that the metal

[redacted]
SIFIED

TABLE VII. EFFECT OF METAL PARTS

Shots Compared	R_n(cased)/R_n(not cased)
RFS-5/RFS-4	1.21
S-6/S-5	1.42
T-9/T-6	1.37
T-12/T-3	1.29
R-13/R-1	2.54
R-13/R-12	2.10

SIFIED
[redacted]

parts do somewhat reduce the degree of breakup of the graphite. Whether in an actual engine the effect would be as pronounced as in the one comparison made on a divided assembly is difficult to estimate.

Only one direct observation was made of the effect of surrounding the high explosive with a metal "shell-case." The comparison of T-4 with T-1 indicates that a 1/32 in. wall copper tube around the Comp B charge reduced R_o by 14%. This difference was not considered significant, and is simply taken to indicate that the addition of a shell-case does not hinder the objective of the program, and may slightly aid it. No consideration of, or compensation for, the existence or nonexistence of a shell case has been made in the comparisons and computations of other factors in the investigation.

V. ESTIMATES OF THE HIGH-EXPLOSIVE FRAGMENTATION OF KIWI CONFIGURATIONS

If one assumes that the actual high-explosive reduction of a NERVA engine results in a fragment distribution of the form employed in this study, then reasonable estimates of the parameters controlling this distribution may be made and order-of-magnitude figures obtained for the degree of destruction of the core.

It seems sensible to apply the truncated distribution expressed in Eq. (8) to describe the fragmentation of a full-scale model. Indeed, if reasonable values for R_o and B are chosen and the distribution is not cut off at a maximum size, one observes that about 10% of the original volume of a B-4 engine would be left in a single piece, a rather unlikely circumstance for a configuration originally composed of approximately two thousand elements of equal size. The principal assumption which must be made in using the cut-off form is that the rules regarding explosive weight, scaling, etc., derived for the nontruncated distribution also apply to the parameters of the truncated one.

Over the range of geometries and scales employed in the experimental program, this assumption appears valid. However, the question remains as to its validity for the much more finely divided geometry of the actual engine configurations.

Before proceeding to the full-scale Kiwi configurations, it is interesting to attempt the "prediction" of the distribution of element fragments in the modular experiment, RFS-10. In the calculation, the rule-of-thumb value of 2/3 was employed for B'. The value of R'_o may be predicted using Eq. (7) and the average value of R_n and R'_n from shots R-3 and R-9. After reducing the value obtained by 20% to allow for the tendency discussed in Section IV-D for "mixed" assemblies, an estimate of R'_o of 1.37 mm was obtained. Finally, an R_{max} corresponding to the second-nearest hole separation (11 mm) was selected. The computed distribution, which was obtained before the actual data were analyzed, is compared with the experimental points and analysis in Fig. 11. As may be seen, the estimate suggests somewhat larger pieces than those obtained, arising largely out of the choice of R'_o, which was only 0.78 mm in the experimental fit. The overestimation of R'_o quite probably arose from the failure of the linear scaling rule, as was noted in the case of

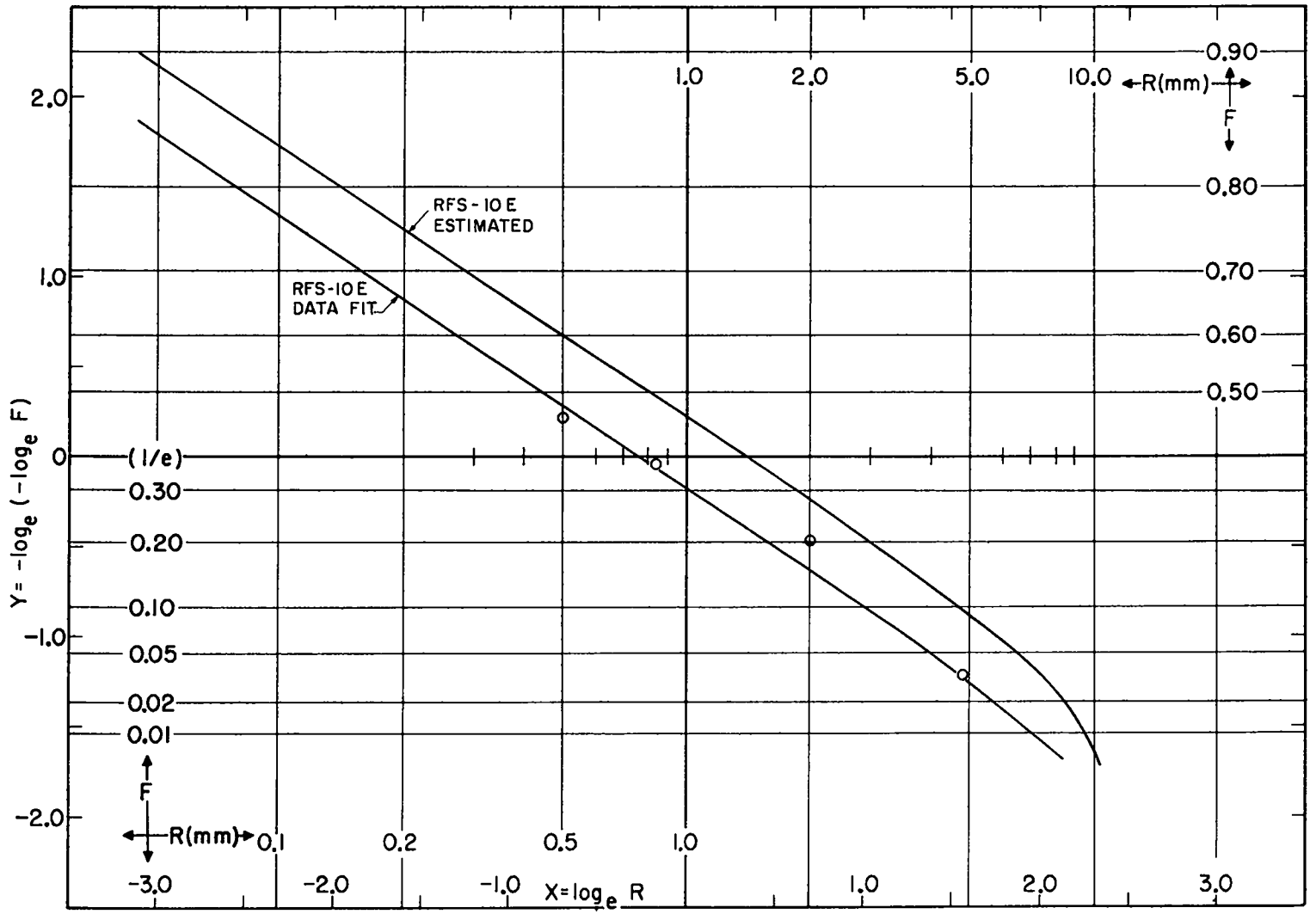

Fig. 11 Comparison of estimated fragment distribution for the fuel element portion of modular assembly RFS-10 with the least squares fit to the recovery data.

the 1/3-scale, 2 in. diam rod assemblies.

Computations were executed for two full-scale Kiwi configurations, the B-1A type arrangement and the B-4 type. The former is an array of 3/4 in. diam, seven-hole fuel elements arranged seven to a Graph-i-tite G Module. The core of the B-4 assembly is composed, except for the central rod of each seven-unit hexagonal array, entirely of 3/4 in. diam, nineteen-hole, hexagonal fuel elements. The entire original volume of each configuration was taken as 10^6 cm^3, with the weight of the loaded graphite, the only part of concern, taken as 7×10^5 gm in the B-1A engine and 10^6 gm in the B-4 assembly. All computations were based on disposal with 100 lb of high explosive. A value of 2/3 was again employed for B'. The definition of R'_n was such that no corrections for scaling and explosive weight were required. Allowing that the "heat treatment" of a run would produce a value of R'_n more like that of the carbided or unloaded elements than that observed for the normal elements fired, a value of 7.5 mm was chosen for the parameter. This figure then multiplied by a factor of two for the presence of the case, and, for the B-1A system, reduced by 20% for the mixed nature of the assembly. In the computations, an example using R'_o = 9 mm was added

[redacted]

to those for R'_o = 12 and 15 mm, which were argued above. The values of R_{max} were chosen on two bases:

1. That the entire diameter of the elements would survive, corresponding to R_{max} = 19 mm;
2. That fragments would be no larger than the second-nearest neighbor distances in the webs of the elements, providing values of 11 mm for the B-1A elements and 7 mm for the B-4 assembly.

The computed results for the nine combinations which arise from the three values each of R'_o and R_{max} are shown graphically in Fig. 12. The four most likely combinations (R'_o = 12 mm, R_{max} = 11 mm or 19 mm for the B-1A assembly; R'_o = 15 mm, R_{max} = 9 mm or 19 mm for the B-4 configuration) are shown in Table VIII. For convenience, the tabulation is in terms of weights rather than fractions and dimensions. The figures mentioned above provided the original weights, and the relation discussed earlier ($R^3 = V$) connected the fragment sizes with the dimension quantities.

[redacted]

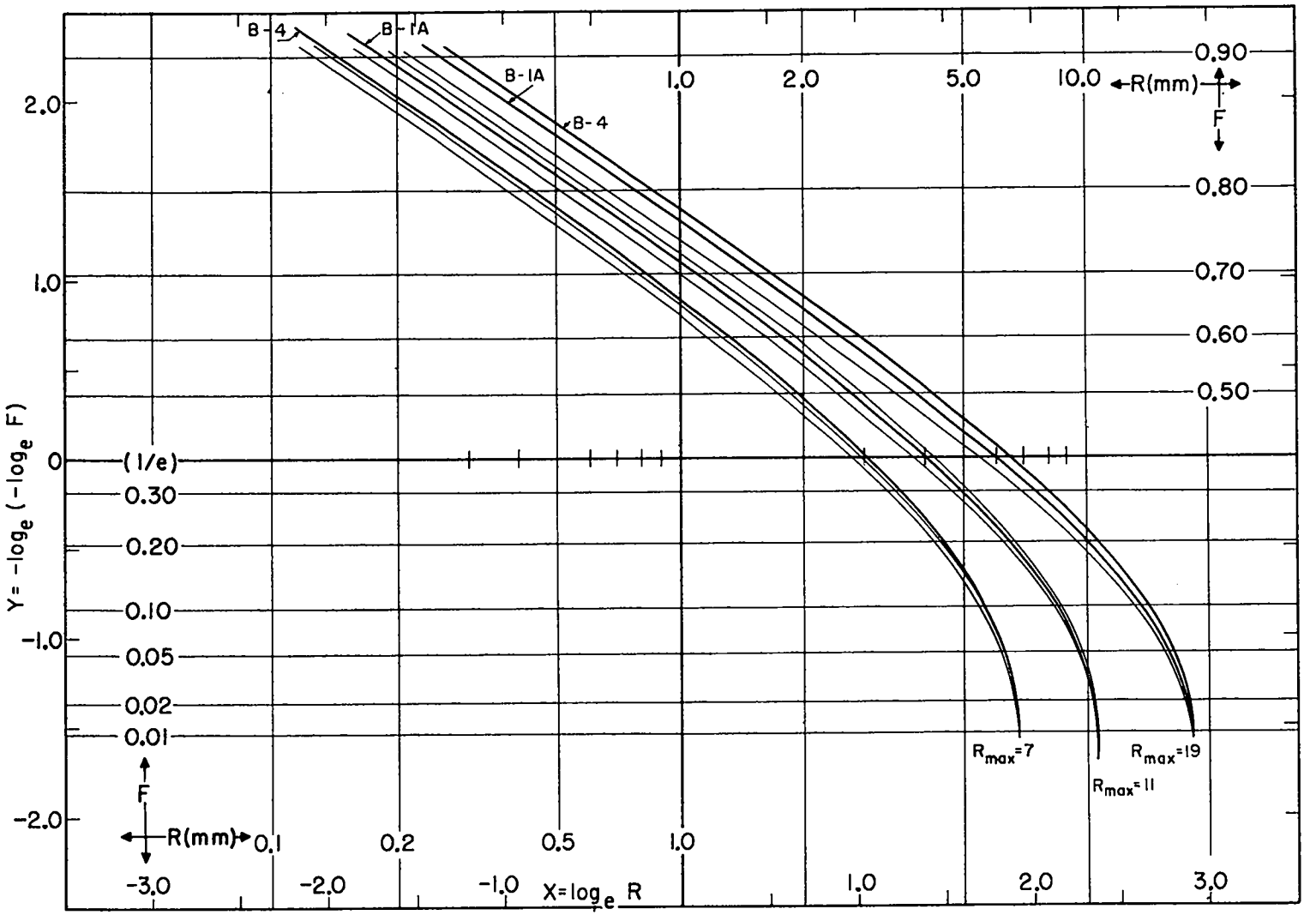

Fig. 12 Estimated range of element portion fragment distributions from the disposal of full-scale Kiwi reactors with 100 lb of high explosive. The nine curves are seen to fall into three sets labeled for R_{max}; within each set the curves, from left to right, are for R_0' equal to 9, 12 and 15 mm. The four heavier curves, labeled B-1A or B-4, correspond to the distributions listed in Table VIII.

APPROVED FOR PUBLIC RELEASE

[redacted]

SECRET

TABLE VIII. ESTIMATES OF FRAGMENTATION OF FULL-SCALE KIWI CONFIGURATIONS WITH 100 LB OF HIGH EXPLOSIVE.

The maximum fragment weights are determined by R_{max} with the assumption $V_{max} = R^3_{max}$. In the computations, the fragment densities were assumed to be 2.15 gm/cm^3 when the pieces were smaller than the second nearest neighbor with sizes. When larger pieces were considered, such that holes were included, "effective" densities of 1.63 gm/cm^3 and 1.47 gm/cm^3 were used for the B-1A and B-4 models, respectively.

Kiwi Model	B-1A		B-4	
Assumed Original Mass of Fuel Element Material (kg)	700		1,000	
Assumed R'_o (mm)	12		15	
Assumed R_{max} (mm)	11	19	7	19
Weight (kg) of material having fragment weights greater than:				
10 gm	none	28	none	2
5	none	81	none	80
2	31	150	none	190
1	91	200	none	270
0.5	160	250	55	380
0.2	230	320	200	480
0.1	280	340	290	540
0.05	340	400	380	590
0.02	390	450	480	660
0.01	430	480	550	700
Maximum Fragment Weight (gm)	2.9	11.2	0.7	10.1

SECRET

VI. SOME CONCLUSIONS AND SUGGESTIONS REGARDING FUTURE WORK

The factors discussed in Section IV may generally be separated into two groups: those important to the degree of fragmentation accomplished in a graphite assembly with centrally located explosive; and those not important. In the former category are scaling, amount of explosive, and the initial geometry of the configuration. Less sensitive factors include the effects of metal parts and variations in the physical properties of the graphite. The type of explosive employed was found, as expected, to have very little effect.

In examining the more important variables, it was observed that a linear scaling rule proved sufficient for prediction of full-scale arrangements. Over a modest range around the 100 lb equivalent explosive weight which has been suggested, it was found that the degree of fragmentation was roughly inversely proportional to the amount of explosive employed. More on the basis of direct observation than of trends in the distribution

parameters, it was concluded that the initial geometry of the system tended to place an upper limit on the size of fragments obtained.

The arguments regarding geometry provided somewhat more optimistic estimates of the fragmentation of the full-scale devices than those which had been accepted earlier. The conclusion was that disposal with 100 lb of explosive would leave virtually no element material in pieces larger than 10 gm, and would reduce the major portion of the reactor core to fragments of less than 2 gm. This estimate was predicated on very consistent observations of maximum fuel element fragment sizes in 1/3- and 1/9-scale shots. No real guarantee can be provided that these observations would prove true in a full-scale experiment; however, common sense suggests that they would.

If the estimates in the previous section, coupled with information about "acceptable" piece sizes (both what could be allowed to reach the earth, and what would burn up on reentering the atmosphere), should indicate the true feasibility of the method; then the most desirable future experiment would be the destruction of a full-scale, detailed device. The design of such an experiment should prove quite simple. Firing the arrangement on a tower in

a large, barren, flat area, with a subsequent sweeping operation, should serve very well. Acquisition of the model would no doubt prove far more difficult, and considerable further work should be done before such an expensive step can really be warranted.

The geometry effect is probably the most uncertain area of the investigation, and that in greatest need of further attention. Kreyenhagen has suggested the possibility of experiments in which only a small sector of the assembly is recovered.[11] These have the immediate advantage that considerable care could be taken in the recovery of the sector, using a sufficiently elaborate means that secondary breakup need be of no concern. With such an arrangement, a full-scale experiment to determine if the complicated element shapes do, indeed, break at the hole sites could be conducted in a fashion which would be relatively economical in critical parts. In such an experiment only the segment to be recovered would need to be composed of element shapes, and stock graphite material, such as 3/4" rods, should serve as an adequate inertial mock-up for the remainder of the system.

The invariable observation from the shots listed in Table II was that the maximum size of element piece recovered was

11. K. N. Kreyenhagen, Private Communication.

determined by the web size. This raises the question of how far the equivalent explosive weight could be reduced without alteration of this fact. Since substantial reduction of the disposal system weight could be effected if a projectile weight reduction could be allowed, further experiments of the type done in this program on the fuel elements are strongly indicated. A recently fired shot, not analyzed with the other data, has demonstrated that a limit of explosive weight exists below which the elements no longer break at every web. A 1/9-scale mixed element (B-1A shapes both loaded and unloaded, and loaded B-4 elements) assembly, similar to those shown in Fig. 4, was fired with the equivalent of 31 lb of explosive. While no intact rod portions were recovered, numerous pieces of all types were found to have included holes. The largest unloaded B-1A piece weighed 17 gm, corresponding to a volume of a cube 22 mm on an edge. The largest fragments of loaded elements in the B-1A and B-4 shapes, respectively, were 12 gm, equivalent to a 19.4 mm cube, and 6 gm representing a cube of dimension 16 mm.

Present disposal schemes include the use of a self-induced after-heat process to reduce the radioactivity of the core before exploding it. This suggests the advisability of an experiment in

which a core model is destroyed while at a high temperature. Such an experiment could prove a bit elaborate; however, present technology would allow, without great difficulty, the design of a simple "air-gun" projector to place the explosive charge in the heated model.

The possibilities of increased fragmentation per pound of explosive through the use of certain aluminized explosives was discussed in Section IV-C. While the advantage accruing from the use of the loaded explosive does not appear substantial, an experimental check of the gain would require very little effort. The present view is that, barring appreciable differences in fragmentation, selection of the type of explosive for an actual system would be dictated by its resistivity to radiation.[11] It could be advisable to include aluminized explosives with those now being tested for nuclear radiation damage.

All the experiments discussed above involve charges extending the entire length of a cylindrical assembly; this requirement seems quite advisable in the design of an actual system. In some early experiments not covered in this report, it was found that charges extending only part of the length of a solid cylinder left an unshattered cone at the end not containing

explosives. It has been reported[11] that disposal mechanisms involving the implanting of several charges in the core are under consideration. Both the scaling rule and an experimental observation in this program (that most of the larger fragments originate from the periphery of the assembly) indicate that such an arrangement would provide greater fragmentation per pound of explosive. A few scaled experiments would be useful to assay the extent of the gain that could be obtained.

Finally, there is considerable area for improvement in the theoretical and computational aspects of the study. The difficulties in the purely empirical use of an unjustified distribution became quite apparent when the question of geometry entered the computations for the full-scale devices. While the principle that enough empirical information could allow reasonable predictions may still be valid, there certainly was not enough data on the geometry effect for this program. Perhaps a better justification of Rosin's Law than the author has observed (which is reputed to exist[11]) would either justify the computational method used, or point the way to a correct one. Also, the original view held in this program, that hydrodynamic calculations of the problem would prove fruitless, should probably be moderated to the attitude that

[redacted]

such an approach might prove helpful. There are now data against which the results of such a study could be compared.

APPENDIX A

DISPERSAL OF ONE-THIRD-SCALE MODELS

Three shots in the program were conducted to obtain information on the manner in which the fragments and debris were dispersed by the explosive. Results from such shots were intended to give a guide to dispersal of engine parts in a possible firing pad accident with NERVA. The purely qualitative observations are presented below.

The recovery phase of these dispersal-recovery shots was accomplished by a sampling technique with tarpaulins on the ground at various distances. Two tarpaulins were located at each of the following distances from the zero-point: 25, 50, 100, 150, 200, 250, 300, 400 and 500 ft. The center of the shot was elevated 3-1/2 ft above the plane of the tarpaulins. The size of each tarpaulin was graduated so as to have its area numerically equal (in square feet) the distance from zero-point in feet.

The mass of fragments recovered at each distance is listed in Table IX. Considering the graduation of the tarpaulin sizes, and assuming angular symmetry, the amounts recovered at each distance represent $2/\pi$ the amount deposited in a zero-point centered, ring-shaped area with a width of 1 ft and radius from zero equal to the distance listed. Integration of the function derived from such consideration to obtain the total mass dispersed generally fell short of original mass by about 20%. This probably indicated a real or virtual loss of finer material, either as smoke, or due to improper construction of the function at distances less than 25 ft.

The shots were also instrumented with upright 4 ft x 8 ft Celotex screens 25, 50, and 100 ft from zero point. The conditions of these screens after the shots are shown in Figs. 13, 14 and 15, and some qualitative remarks are made in the figure captions.

A further qualitative observation may be made regarding the tarpaulin recoveries. The zero values shown in Table IX at distances of 400 and 500 ft do not indicate that no fragments attained that distance; pieces, but very few of them, were found at distances exceeding 500 ft. The tarpaulin data, as well as those from the screens, indicated a decided distribution of

[redacted]
SIFTED

TABLE IX. DISPERSAL DATA FROM DISPERSAL-RECOVERY SHOTS

The sizes of samples taken at various distances are discussed in the text.

Shot Number	RFS-4	RFS-5	RFS-6
Graphite Mass (kg)	60.8	58.1	68.2
Graphite Configuration	Solid Cyl.	Solid Cyl.	Modular
Cased	No	Yes	Yes
High-Explosive Mass (kg)	1.75	1.69	1.70
Dispersal Data: Mass (gm) of graphite recovered at distance of:			
25 ft	21	101	68
50 ft	78	70	151
100 ft	57	77	110
150 ft	48	32	67
200 ft	43	31	18
250 ft	24	11	5
300 ft	16	10	9
400 ft	3	0	0
500 ft	0	0	0

Fig. 13 Screen penetration from shot RFS-4. The setup, with tarpaulins and screens, is shown in the upper left. The screens shown in the other panels are labeled as to distance, in feet, from the shot. As would be expected, the density of fragments impacting the screens is substantially reduced at greater distances, by more than the factor of four expected for comparison of the 25 ft and 100 ft distances. (Due to the cylindrical geometry, it is the plane, and not the solid angle which should be considered.) It may be noted that at greater distances only the larger pieces penetrate the single layer of 1/2" Celotex.

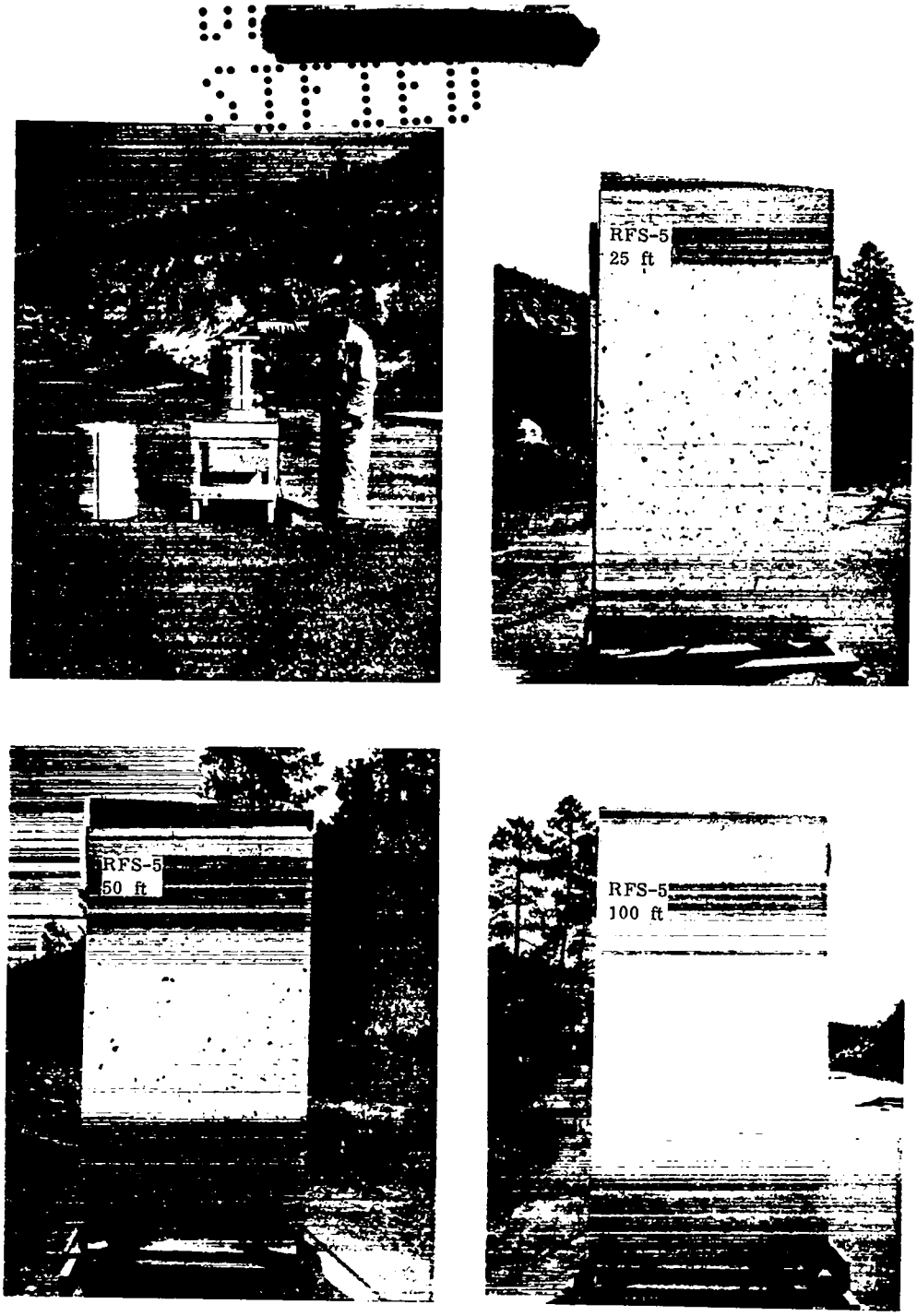

Fig. 14 Screen penetration from shot RFS-5. This shot was virtually identical to RFS-4, except that simulated metal parts were employed around the solid graphite cylinders. Comparison with Fig. 13 shows that the confining effect of the case mock-up served to substantially reduce the number of graphite pieces sticking to or penetrating the screens at all distances.

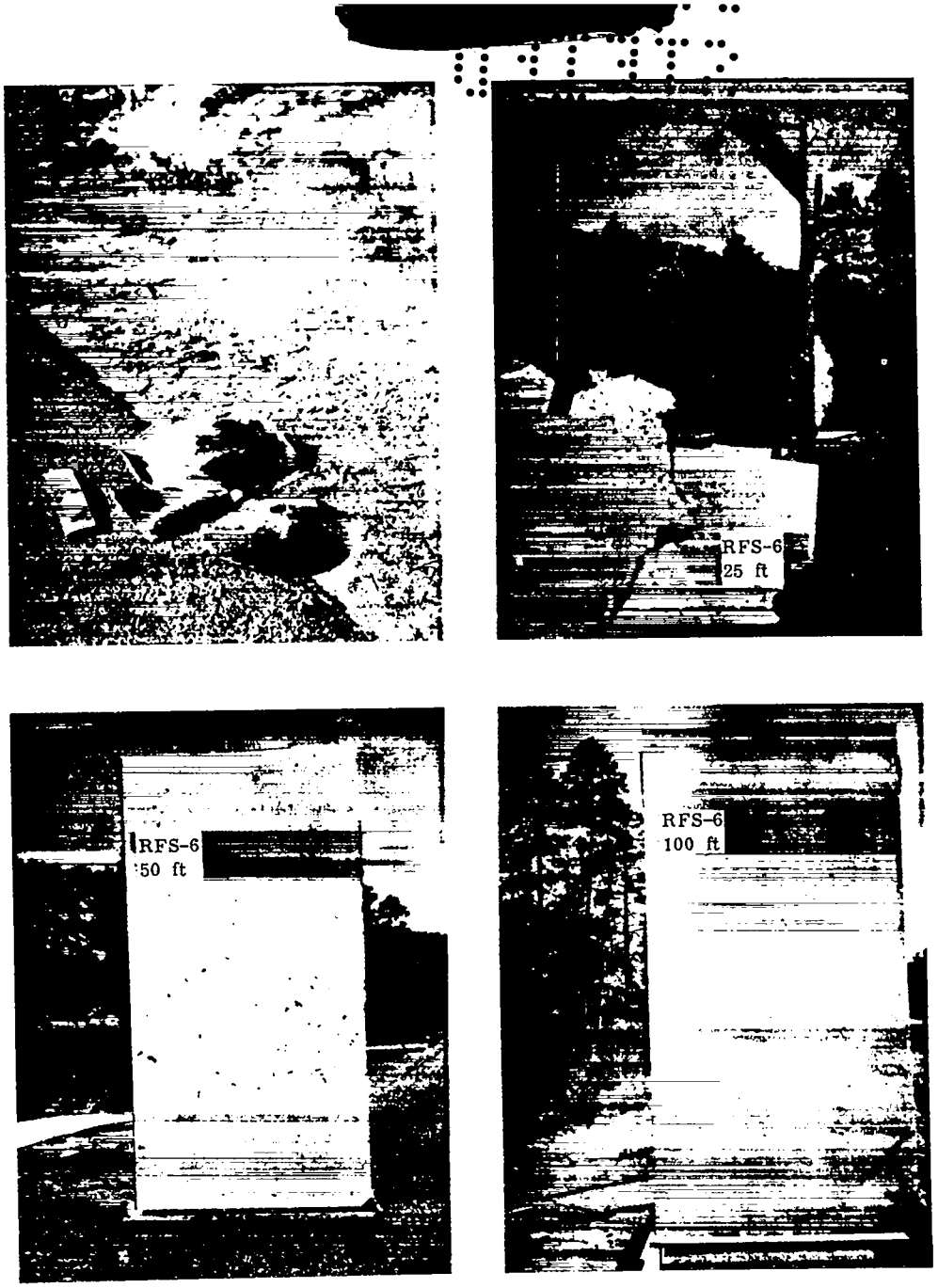

Fig. 15 Screen penetration from shot RFS-6. It is interesting to note the penetration of the 25-ft screen by one of the bars representing the reflector. The bar was apparently in an upright position, as indeed all of them generally appear to be in Fastax pictures. The upper left panel of the figure shows some recovered pieces of the reflector and pressure-shell model.

larger fragments at greater distances. This was assumed to be primarily due to greater relative atmospheric drag on the smaller pieces.

The pressure shell mock-ups were broken into 5 to 10 pieces, which were recovered at distances of 200 to 500 ft from zero point. The Duralumin bars representing the reflector system were recovered unbroken at similar distances. It seems likely that the reflector model would have shattered, had it been extensively tubulated beryllium rather than solid Duralumin.

Fastax studies of the shots indicated that a small portion of the graphite was projected upward, but the greater portion left the explosion site radially. The principal motion of the metal parts was also radial, with virtually no tumbling of the reflector bars. The initial velocity of the metal parts from the cased assemblies was about 600 ft/sec, with the graphite following behind. In the uncased shot, the graphite pieces were observed to have a maximum initial velocity of about 900 ft/sec.

APPENDIX B

A SIMPLE FRAGMENTATION DISTRIBUTION

I. Introduction

An attempt is made in this appendix to obtain from probability arguments and a simple assumption (that a probability per unit length exists for a separation plane) a form for the expected distribution of fractional total volume in particle size. The form will be the result of a "single shattering process".

II. The Linear Problem

We shall first treat the problem in detail in one dimension, since with some simple assumptions, this problem permits an easy generalization to the full three-dimensional one.

Our experiment consists of taking a stick of length L and shattering it. There will result n pieces, of length x_1, x_2, ... x_n. Thus, our sample space consists of the discrete random variable n, and for each n we have n-1 continuous variables, $x_1 \ldots x_{n-1}$, the variable x_n being fixed by the constraint $x_1 + \ldots + x_n = L$.

To obtain the probability density, $P(n; x_1, \ldots, x_{n-1})$, we need to make some assumption about the way the stick breaks. Our fundamental assumption is that there is a probability, α, per unit length of breaking, and that this probability is independent of position on the stick.

Now $P(n; x_1 \ldots x_{n-1})\, dx_1 \ldots dx_{n-1}$ equals: (probability of no break in x_1) x (probability of break in dx_1) x ... . For the probability of no break in x_1 we have

$$\text{Lim } (1-\alpha\Delta x)^{(x_1/\Delta x)} = e^{-\alpha x_1} .$$

Hence,

$$P(n; x_1 \ldots x_{n-1}) = e^{-\alpha x_1} \alpha dx_1 \, e^{-\alpha x_2} \ldots \alpha dx_{n-1} \, e^{-\alpha x_n} \tag{1}$$

if $\sum x \leq L$ and is 0 otherwise.

The probability of having n pieces is obtained by integrating $dx_1 \ldots dx_{n-1}$

$$P(n) = \int_0^L dx_1 \int_0^{L-x_1} dx_2 \int_0^{L-x_1-x_2} dx_3 \ldots \int_0^{L-x_1 \ldots -x_{n-2}} dx_{n-1} \; P(n, x_1 \ldots x_{n-1}). \tag{2}$$

[redacted]

These integrals may be done by recognizing the recursive nature of each intermediate integration. That is, we have the form

$$\int_0^{a_p} dx(a_p - x)^{p-1}/(p-1)! = a_p^p/p! \quad , \tag{3}$$

and p is the number of integrations performed, and a_p is the upper limit of the last integration. This simplification occurs only because we made the simplest of possible assumptions about α.

We have

$$P(n) = \frac{(\alpha L)^{n-1}}{(n-1)!} e^{-\alpha L} \quad , \tag{4}$$

$$\sum_{n=1}^{\infty} P(n) = 1 \quad , \tag{5}$$

$$\sum_{n=1}^{\infty} nP(n) = 1 + \alpha L \quad . \tag{6}$$

[redacted]

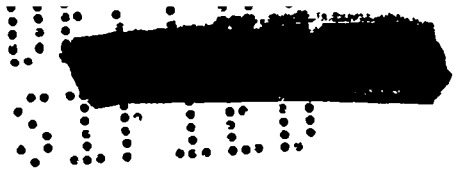

Thus n has a Poisson distribution, as might be expected.

We can also calculate the joint probability of n and x (where x is any of the $x_1 \ldots x_n$) and the probability of x by integrating or summing over the other variables. This yields

$$P(n, x) = \alpha e^{-\alpha L} \frac{(\alpha L - \alpha x)^{n-2}}{(n-2)!}, \qquad n \geq 2,$$
$$= e^{-\alpha L} \delta(x-L), \qquad n = 1, \tag{7}$$

$$P(x) = \alpha e^{-\alpha x} + e^{-\alpha L} \delta(x-L). \tag{8}$$

The conditional probability, $P(n,x)/P(n)$, corresponds to the probability that a piece selected at random will have length x, given that n pieces resulted from breaking the stick. P(x) is the same probability without any condition on n.

We now consider the analogue in one dimension of the screening process in three dimensions. Given an n, $x_1 \ldots x_{n-1}$ point in sample space, we can construct a function $g(\bar{x}, n, x_1 \ldots x_{n-1})$ which gives the fraction of total length of pieces that have length greater than $\bar{x}$.

[redacted]

$$g(\bar{x},\, n,\, x_1 \ldots x_{n-1}) = \frac{1}{L} \sum_{x_i > \bar{x}} x_i$$

$$= \frac{1}{L} \sum_{i=1}^{n} x_i \theta(x_i - \bar{x}), \qquad (9)$$

where $\theta(x) = 1\ (0)$ if $x > 0$ (<0).

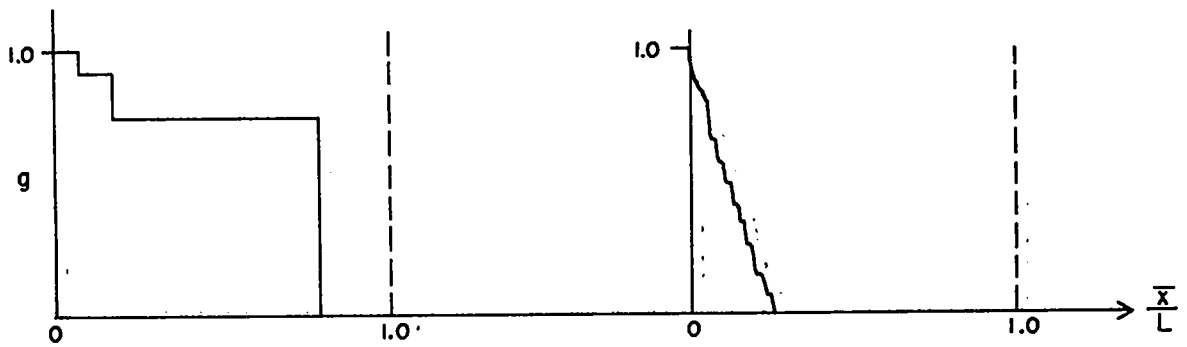

Fig. 16 Examples of g for specific sample points

Two such g-functions are shown in Fig. 16. If αL is large, the first one shown has small probability. It is only for large numbers of particles that g approaches a continuous function. Since this is the case in which we shall be interested, we can

[redacted]

compute the expected value of this function by weighting the g's by $P(n, x_1 \ldots x_{n-1})$ and averaging over the sample space. We have

$$g(\bar{x}) = \sum_{n=1} dx_1 \ldots dx_{n-1}\, g(\bar{x}, n, x_1 \ldots x_{n-1})\, P(n; x_1 \ldots x_{n-1})$$

$$= \sum_{n=1} \frac{n}{L} e^{-\alpha L} \alpha^{n-1} \int_0^L dx_1\, x_1\, \theta(x_1 - \bar{x}) \int_0^{L-x_1} dx_2 \ldots \int_0^{L-x_1 \ldots -x_{n-2}} dx_{n-1}$$

$$= \sum_{n=1} \frac{n}{L} e^{-\alpha L} \alpha^{n-1} \left\{ \frac{(L-\bar{x})^n}{n} + \frac{\bar{x}(L-\bar{x})^{n-1}}{(n-1)!} \right\} \qquad (10)$$

$$= e^{-\alpha \bar{x}} \left[1 + \alpha \bar{x} \left(1 - \frac{\bar{x}}{L} \right) \right] .$$

Note that this $g(\bar{x})$ differs from the probability that one piece selected at random has size greater than $\bar{x}$. This probability is simply $\int_{\bar{x}}^{L} P(x)dx \approx e^{-\alpha \bar{x}}$.

III. The 3-Dimensional Problem

We consider a cube LxLxL and assume that the previous analysis applies to each axis of the cube. The parameter α becomes the probability of the occurrence of a separation plane per unit length. Thus a point Q in sample space (discrete variables $n_x\ n_y\ n_z$; continuous variables $x_1 \ldots x_{n_x-1}$; $y_1 \ldots y_{n_y-1}$; $z_1 \ldots z_{n_z-1}$) corresponds to reducing the cube to a rubble of rectangular pieces. The amount of new area produced in this

rubbling process is simply

$$A = (n_x - 1)\, L^2 + (n_y - 1)\, L^2 + (n_z - 1)\, L^2 . \qquad (11)$$

From (6), the expectation value of n-1 is simply αL. We then give another meaning to α from $A = 3\,\alpha L^3$.

$$\alpha = \frac{1}{3} \text{ area produced per unit volume.} \qquad (12)$$

The assumption of orthogonal separation planes should not be too bad if the major part of the rubble is in small pieces. In terms of short-range order, the probability that the angle between two intersecting separation planes is in the vicinity of 90° is much greater than the probability for small angles. The long range orthogonality is simply a means of simplifying calculations. If one were dealing with a single crystal, one would choose the three (or more) most easily cleaved crystal planes and probably get reasonable answers.

Since the probabilities in the three directions are separable, the probability of a point Q in permissible sample space (permissible means Σx, Σy, $\Sigma z < L$) is the product of the probability densities we obtained for the one-dimensional case

$$P(Q) = e^{-3\alpha L}\, \alpha^{n_x+n_y+n_z-3} . \tag{13}$$

Similarly we have from (7) and (8)

$$P(n_x n_y n_z, xyz) = P(n_x, x)\, P(n_y, y)\, P(n_z, z) , \tag{14}$$

$$P(xyz) \approx \alpha^3 e^{-\alpha(x+y+z)} . \tag{15}$$

We now construct a function g(v, Q) which gives, for each point in the sample space, the fraction of the total volume that resides in particles whose volume is greater than or equal to v.

$$\begin{aligned} g(v,Q) &= \frac{1}{L^3} \sum_{\substack{\text{all particles} \\ \text{for which } xyz > v}} xyz \\ &= \frac{1}{L^3} \sum_{i,j,k=1}^{n_x n_y n_z} x_i y_i z_k \theta(x_i y_j z_k - v). \end{aligned} \tag{16}$$

Again we are interested in the case where the number of particles is large and a particular g(v, Q) resulting from an experiment is likely to be near the continuous function g(v) which is the expectation value of g(v, Q). We have

$$g(v) = \int dQ\; g(v,Q)\, P(Q) . \tag{17}$$

The integration, unlike the probability density, does not separate because of the presence of the choice function, $\theta(xyz-v)$. However, each of the terms in the sum (16) gives a like contribution, and we pick up a factor $n_x n_y n_z$. We choose $\theta(x_1 y_1 z_1 - v)$ $x_1 y_1 z_1$ as the typical term and obtain

$$g(v) = \frac{1}{L^3} \sum_{n_x n_y n_z} n_x n_y n_z \int_0^L dxdydz\ xyz\ \theta(xyz-v)\ P(n_x n_y n_z,\ xyz)\ . \tag{18}$$

The n-sums can be done to give

$$g(v) = \frac{1}{L^3} \int_0^L dxdydz\ xyz\ \theta(xyz-v)\ f(x)\ f(y)\ f(z)\ ,$$

$$f(x) = e^{-\alpha x} \left[\alpha^2 (L-x) + 2\alpha + \delta\ (x-L) \right]\ . \tag{19}$$

We shall be interested in the case where we have a large number of particles (α L >> 1). This limit can be conveniently obtained from (19) by L $\rightarrow$ ∞. We then have

$$g(v) = \int_0^\infty dxdydz\ \alpha^6\ xyz\ \theta(xyz-v) e^{-\alpha(x+y+z)}\ . \tag{20}$$

We now define a mean dimension r and a dimensionless parameter η proportional to the mean dimension.

$$r = v^{1/3} . \tag{21}$$

$$\eta = \alpha r . \tag{22}$$

If we make these substitutions in (20) and let $\alpha x \rightarrow x$, we obtain a universal function, $g(\eta)$, to describe the volume fraction. Thus α enters as a scaling parameter on the mean dimension of a particle for the case where $\alpha L \gg 1$. We have

$$g(\eta) = \int_0^\infty dxdydz\ \theta(xyz-\eta^3)\ e^{-(x+y+z)}\ xyz . \tag{23}$$

The z-integration can be done

$$g(\eta) = \int_0^\infty dxdy\ (xy + \eta^3)\ e^{-(x+y+\eta^3/xy)} . \tag{24}$$

If one uses $x = r \cos(\phi/2)$, $y = r \sin(\phi/2)$, this may be transformed into:

$$g(\eta) = \int_0^\infty dr \int_0^{\pi/2} d\phi\ r\ (r^2 \sin\phi/2 + \eta^3)\ e^{-r(1+\sin\phi)^{1/2} - 2\eta^3/(r^2 \sin\phi)} \tag{25}$$

a form suitable for numerical integration.

The function $g(\eta)$ was computed in the r, ϕ plane using Simpson's rule in the regions of maximum contribution. It is

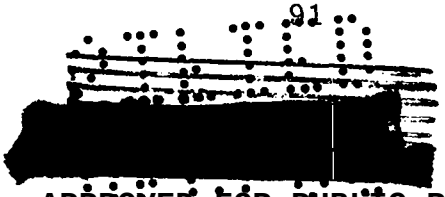

listed in tabular form in Table X and shown in Figs. 17 and 18.

IV. Comparison with Experimental Results (Qualitative)

If we try to scale experimental data to obtain a best fit to Fig. 17, we find in general that the theoretical g(x) is too steep, and that the data for the most part fall in a broad band cutting the theoretical curve at the 50% level (a result of scaling) and having approximately half the slope of the theoretical curve.

These features can probably be traced to the neglect of (1) an α that varies radially because of the radial decay of the pressure wave and (2) the abrasion and secondary breakage that occur from the tumbling about and impacts created by the outpouring of the explosive gases after the explosion proper. Both of these effects, if somehow incorporated in the theoretical curve, would cause the theoretical g(x) to flatten out in better agreement with the experimental data.

In particular, effect (2) above should be more noticeable in a geometry of many small parts when compared to a solid configuration. This is indeed found to be the case, the former giving a considerably flatter curve.

These effects could be incorporated by (1) assuming an $\alpha(r)$ to vary as the radial stress, and then taking a weighted

TABLE X. THE INTEGRATED VOLUME DISTRIBUTION FUNCTION, $g(\eta)$

η	$g(\eta)$	$-\ln g$
0.1	0.99501	0.0050
0.2	0.99483	0.0052
0.3	0.99344	0.0066
0.4	0.98908	0.0110
0.5	0.97975	0.0205
0.6	0.96377	0.0369
0.7	0.94009	0.0618
0.8	0.90840	0.0961
0.9	0.86911	0.1403
1.0	0.82314	0.1946
1.1	0.77183	0.2590
1.2	0.71668	0.3331
1.3	0.65925	0.4166
1.4	0.60102	0.5091
1.5	0.54331	0.6101
1.6	0.48723	0.7190
1.7	0.43367	0.8355
1.8	0.38327	0.9590
1.9	0.33649	1.0892
2.0	0.29358	1.2256
2.1	0.25465	1.3679
2.2	0.21968	1.5156
2.3	0.18853	1.6685
2.4	0.16101	1.8263
2.5	0.13689	1.9886
2.6	0.11587	2.1553
2.7	0.09769	2.3260
2.8	0.08204	2.5006
2.9	0.06865	2.6788
3.0	0.05725	2.8604
3.1	0.04758	3.0453
3.2	0.03942	3.2333
3.3	0.03257	3.4243
3.4	0.02683	3.6181
3.5	0.02205	3.8145
3.6	0.01807	4.0135
3.7	0.01477	4.2149
3.8	0.01205	4.4187
3.9	0.00981	4.6247
4.0	0.00796	4.8328

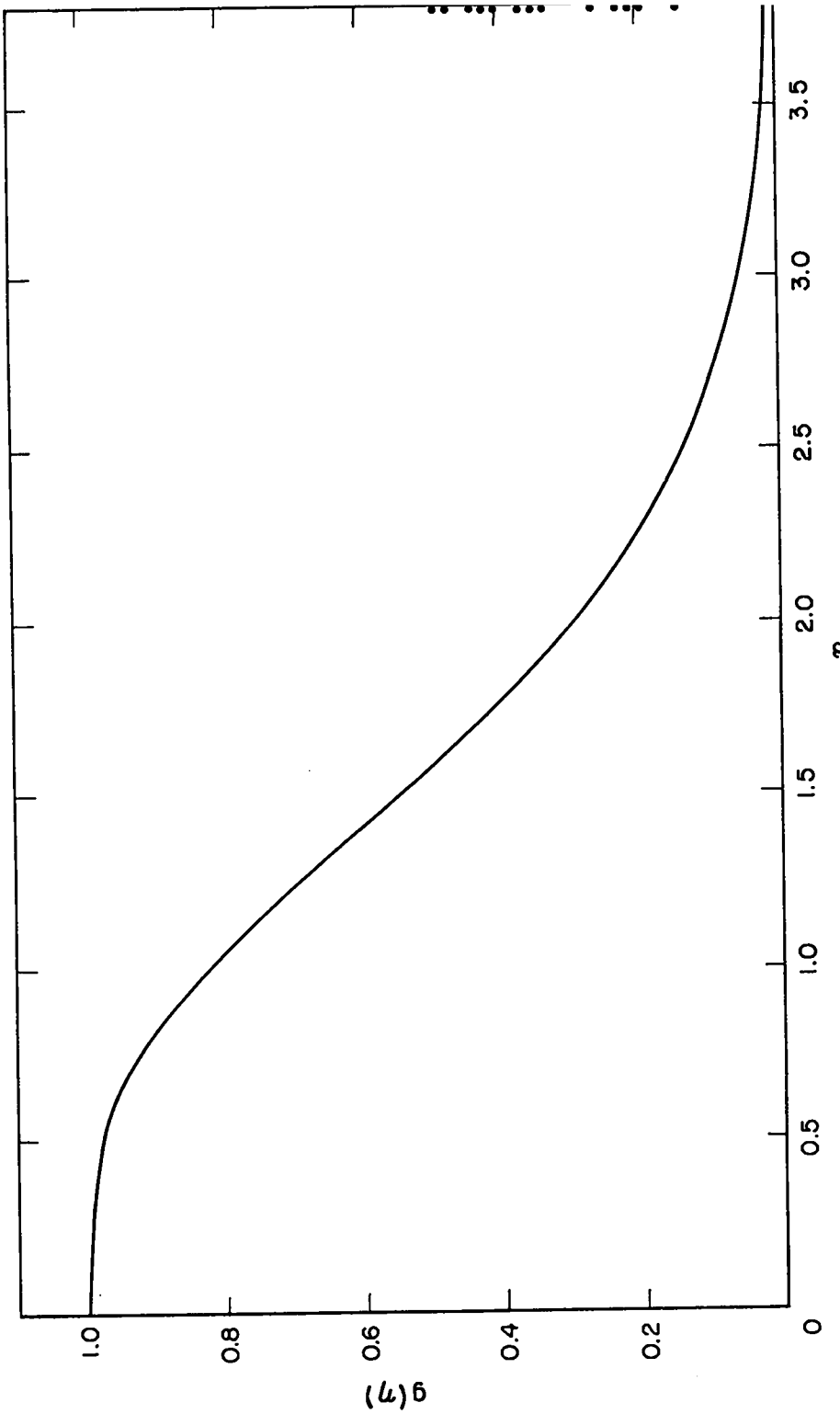

Fig. 17 $g(\eta)$ vs. η.

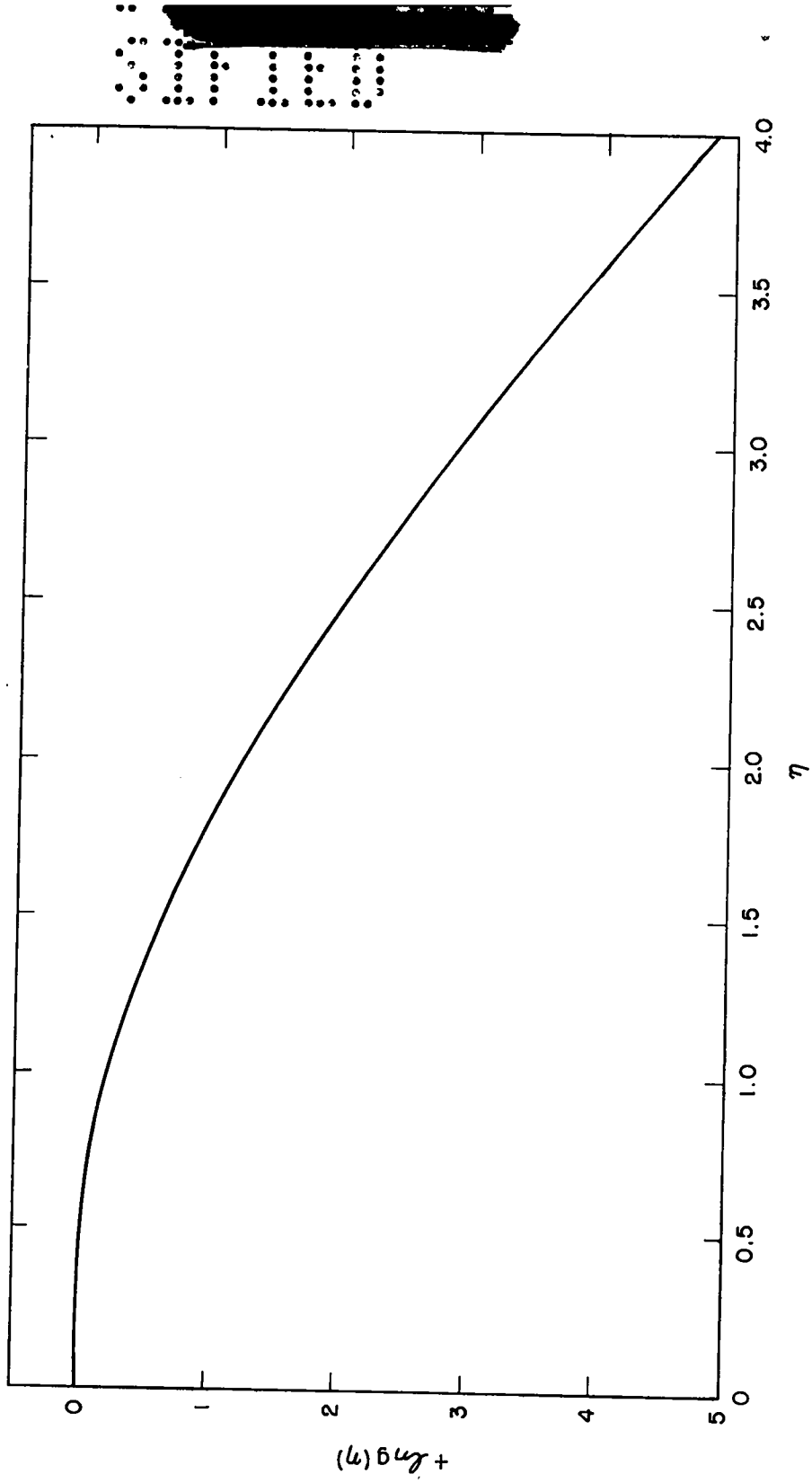

Fig. 18 ln g(η) vs. η

average of g(x)'s, and (2) assuming that each of the rectangular parallelepipeds considered is abraded to an ellipsoid, or broken in half if the longest dimension exceeds some factor of the smallest diameter. In view of the unpromising nature of such assumptions, the fit of the data has been left to the semi-empirical Rosin's Law. In Fig. 19, the theoretical curve $g(\eta)$ has been plotted in a fashion to permit direct comparison with the shapes that Wackerle obtains from his experimental data. For the purposes of plotting, a value for α of 1.8 planes per mm was chosen. Note that in this appendix the function $g(\eta)$ corresponds to Wackerle's F.

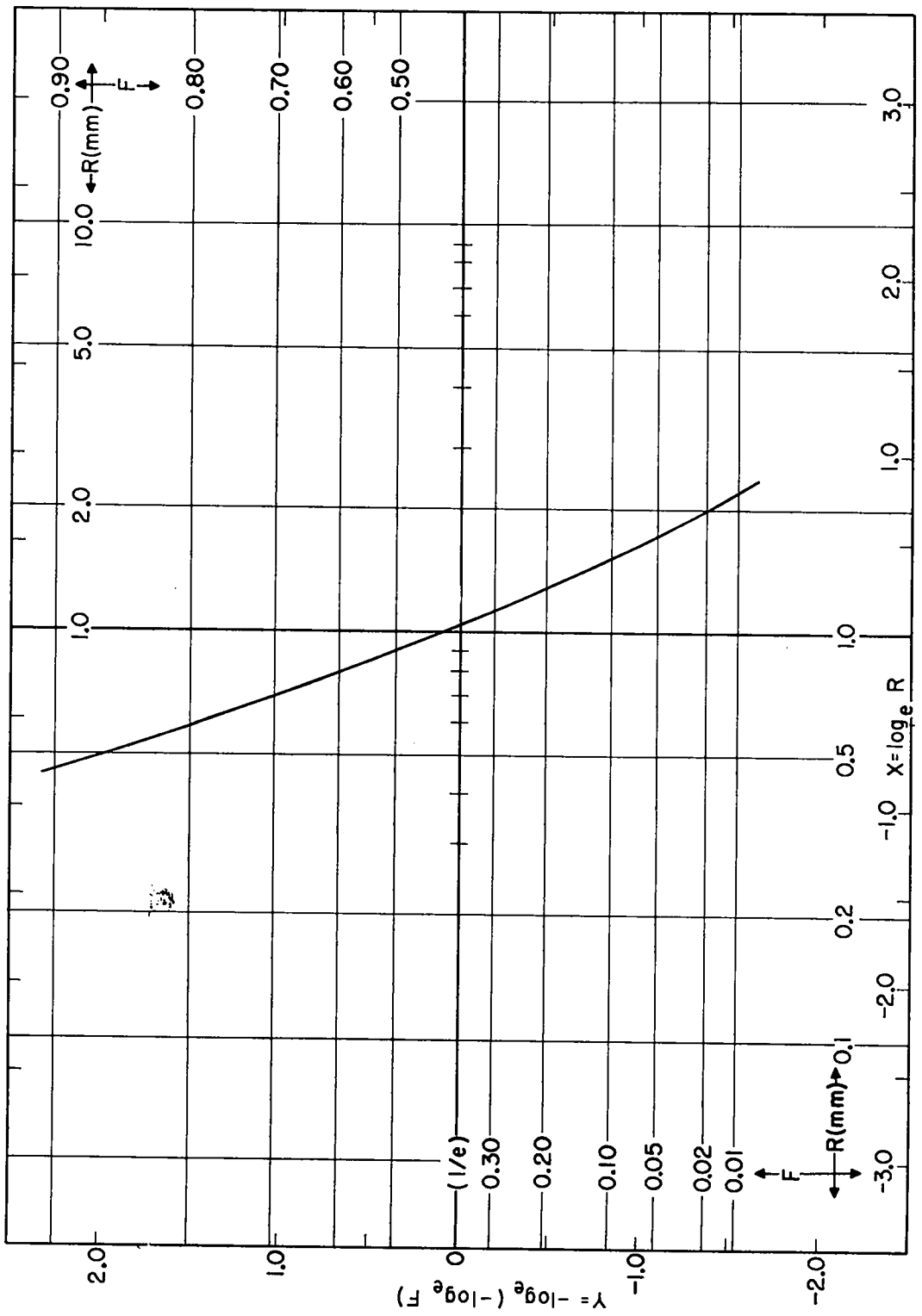

Fig. 19 $-\ln\left[-\ln g(R)\right]$ vs $\ln R$ with $\alpha = 1.8/\text{mm}$

UNCLASSIFIED